



The Asian monsoon
anticyclone in
summer 2012

B. Vogel et al.

This discussion paper is/has been under review for the journal Atmospheric Chemistry and Physics (ACP). Please refer to the corresponding final paper in ACP if available.

Impact of different Asian source regions on the composition of the Asian monsoon anticyclone and on the extratropical lowermost stratosphere

B. Vogel, G. Günther, R. Müller, J.-U. Groß, and M. Riese

Forschungszentrum Jülich, Institute of Energy and Climate Research – Stratosphere (IEK-7), Jülich, Germany

Received: 10 February 2015 – Accepted: 18 March 2015 – Published: 2 April 2015

Correspondence to: B. Vogel (b.vogel@fz-juelich.de)

Published by Copernicus Publications on behalf of the European Geosciences Union.

Title Page

Abstract

Introduction

Conclusions

References

Tables

Figures



Back

Close

Full Screen / Esc

Printer-friendly Version

Interactive Discussion



Abstract

The impact of different boundary layer source regions in Asia on the chemical composition of the Asian monsoon anticyclone, considering its intraseasonal variability in 2012, is analysed by CLaMS simulations using artificial emission tracers. Our simulations show that the Asian monsoon anticyclone is highly variable in location and shape and oscillates between 2 states: first a symmetric anticyclone and second, an asymmetric anticyclone either elongated or split in two smaller anticyclones. A maximum in the distribution of air originating from Indian/Chinese boundary layer sources is usually found in the core of the symmetric anticyclone, in contrast the asymmetric state is characterised by a double peak structure in the horizontal distribution of air originating from India and China. The simulated horizontal distribution of artificial emission tracers for India/China is in agreement with patterns found in satellite measurements of O₃ and CO by the Aura Microwave Limb Sounder (MLS). The contribution of different boundary source regions to the Asian monsoon anticyclone strongly depends on its intraseasonal variability and is therefore more complex than hitherto believed, but in general the highest contributions are from North India and Southeast Asia at 380 K. In the early (June to mid-July) and late (mid-August to October) period of the monsoon 2012, contributions of emissions from Southeast Asia are highest and in the intervening period (\approx mid-July to mid-August) emissions from North India have the largest impact. Further, our simulations confirm that the thermal tropopause above the anticyclone constitutes a vertical transport barrier. Enhanced contributions of emission tracers for Asia are found at the northern flank of the Asian monsoon anticyclone between double tropopauses indicating an isentropic transport from the anticyclone into the lowermost stratosphere.

After the breakup of the anticyclone, significant contributions of air masses originating in India/China are still found over Asia in September/October. In addition, these air masses spread out within the mid-latitudes of the Northern Hemisphere and in the tropics at around 380 K. Moreover, air masses from Southeast Asia experienced diabatic

The Asian monsoon anticyclone in summer 2012

B. Vogel et al.

Title Page

Abstract

Introduction

Conclusions

References

Tables

Figures



Back

Close

Full Screen / Esc

Printer-friendly Version

Interactive Discussion



upward transport in the tropics and subsequently isentropic poleward transport occurs at around 380 K with the result that the extratropical lowermost stratosphere is flooded by end of September with air masses originating in Southeast Asia. Our results demonstrate that emissions from Asia have a significant impact on the chemical compositions of the lowermost stratosphere of the Northern Hemisphere in particular after the end of the monsoon season in September/October 2012.

1 Introduction

The Asian summer monsoon circulation is an important global circulation system in northern summer associated with strong upward transport of tropospheric source gases into the upper troposphere and lower stratosphere (UTLS) region (e.g. Li et al., 2005; Randel and Park, 2006; Park et al., 2007, 2008, 2009). Satellite measurements show that tropospheric trace gases such as water vapour (H₂O), carbon monoxide (CO), nitrogen oxides (NO_x), Peroxyacetyl nitrate (PAN), hydrogen cyanide (HCN), and aerosol are confined by the strong anticyclonic circulation in the UTLS and therefore are isolated from the surrounding air (Rosenlof et al., 1997; Jackson et al., 1998; Park et al., 2004, 2008; Li et al., 2005; Xiong et al., 2009; Randel et al., 2010; Vernier et al., 2011; Bourassa et al., 2012; Fadnavis et al., 2013, 2014). In contrast, stratospheric trace gases such as O₃, HNO₃, or HCl show low concentrations in the anticyclone (Randel and Park, 2006; Park et al., 2008; Liu et al., 2009; Konopka et al., 2010). In general, the Asian monsoon circulation provides an effective pathway for water vapour and pollutants to the lower stratosphere of the Northern Hemisphere (Bian et al., 2012; Ploeger et al., 2013; Vogel et al., 2014; Uma et al., 2014). However, the mechanisms for transport into the lowermost stratosphere are subject of a longstanding debate (Dethof et al., 1999; Park et al., 2009; Randel et al., 2010; Bourassa et al., 2012; Fairlie et al., 2014; Fromm et al., 2014; Vogel et al., 2014).

Increasing stratospheric water vapour have a significant influence on the climate system (e.g. Forster and Shine, 1999; Shindell, 2001; Smith et al., 2001; Forster and

The Asian monsoon anticyclone in summer 2012

B. Vogel et al.

Title Page

Abstract

Introduction

Conclusions

References

Tables

Figures



Back

Close

Full Screen / Esc

Printer-friendly Version

Interactive Discussion



The Asian monsoon anticyclone in summer 2012

B. Vogel et al.

Title Page

Abstract

Introduction

Conclusions

References

Tables

Figures



Back

Close

Full Screen / Esc

Printer-friendly Version

Interactive Discussion



Shine, 2002; Vogel et al., 2012), in particular the variability of water vapour in the lower stratosphere is an important driver of surface climate change (e.g. Solomon et al., 2010; Riese et al., 2012). In addition, increasing stratospheric water vapour plays a crucial role in stratospheric chemistry (e.g. Kirk-Davidoff et al., 1999; Dvortsov and Solomon, 2001; Vogel et al., 2011a). Therefore, it is important to understand transport processes from the Asian monsoon region into the global lower stratosphere.

Moreover, the contribution of different boundary source regions in Asia to the chemical composition of the Asian monsoon anticyclone (e.g. Li et al., 2005; Park et al., 2009; Chen et al., 2012; Bergman et al., 2013; Fadnavis et al., 2014) is currently discussed. Chen et al. (2012) found that most impact at tropopause heights is from emissions originating in the tropical Western Pacific region and the South China Sea, while Bergman et al. (2013) found that air masses originating at the Tibetan Plateau and in India are most important at 100 hPa. Simulations with a chemistry transport model by Park et al. (2009) show that the main surface sources of CO in the Asian monsoon anticyclone are from India and Southeast Asia, whereby the weak contribution of air masses originating from the Tibetan plateau in their analysis is due to the lack of significant surface emissions of CO in this region. Further, air masses from northeast India and southwest China uplifted at the eastern side of the anticyclone could also contribute to the chemical composition of the Asian monsoon anticyclone (Li et al., 2005).

In addition to the impact on the contribution of the Asian monsoon anticyclone, deep convection at the eastern/southeastern side of the Asian monsoon anticyclone can directly transport tropospheric air into the lower stratosphere by direct convective injection (Rosenlof et al., 1997; Park et al., 2007, 2008; Chen et al., 2012). However, the impact of this transport mechanism on the chemical composition of the lower stratosphere has not been isolated from the exchange between the troposphere and the stratosphere associated with the large-scale Brewer–Dobson circulation (Gettelman et al., 2004; Bannister et al., 2004).

The monsoon and the associated seasonal change of wind and rainfall is characterised by prolonged periods of dry and wet conditions in the range of 2–3 weeks. Ex-

The Asian monsoon anticyclone in summer 2012

B. Vogel et al.

Title Page

Abstract

Introduction

Conclusions

References

Tables

Figures



Back

Close

Full Screen / Esc

Printer-friendly Version

Interactive Discussion



tended periods with enhanced precipitation (wet spells) characterise active conditions, while dry spells represent periods when a break in monsoon activity occurs (Goswami, 2012, and references therein). The active and break phases are manifestations of the superposition of large scale northward moving 30 to 60 day oscillations and small scale westward propagating 10 to 20 day variations, however the detailed understanding of the variability is a open question (Goswami, 2012, and references therein). This intraseasonal variability of the monsoon is associated with the strength of the Asian monsoon anticyclone in the UTLS (Goswami, 2012). Therefore, the evolution over the monsoon season of the anticyclone is characterised by large variability in its extent, strength and location (e.g. Randel and Park, 2006). Garny and Randel (2013) found that the temporal variability of the strength of the anticyclone, as diagnosed by low areas of potential vorticity (PV), is driven by the variability in convection with a period of 30–40 days.

Further, westward transport of low PV values or smaller anticyclones separated from the Asian monsoon anticyclone (referred to as “eddy shedding”) occurs more often than the process of eastward migrating smaller anticyclones during the monsoon season (Hsu and Plumb, 2001; Popovic and Plumb, 2001; Garny and Randel, 2013). Moreover, also splittings of the Asian monsoon anticyclone into two separate smaller anticyclones frequently occur each year (e.g. Garny and Randel, 2013). Zhang et al. (2002) report that the longitudinal location of the core of the Asian monsoon anticyclone has two preferred regions, referred to as Tibetan Mode and Iranian Mode, affecting the distribution of chemical constituents in the UTLS (Yan et al., 2011).

In this paper, we investigate what is the impact of different boundary layer sources regions in Asia on the composition of air in the Asian monsoon anticyclone considering the intraseasonal variability of the anticyclone. Further, we analyse how both boundary layer sources regions in Asia and the Asian monsoon anticyclone affect the chemical composition of the lowermost stratosphere for the example of the year 2012.

To answer these questions, we perform simulations with the three-dimensional Lagrangian chemistry transport model (CLaMS) (McKenna et al., 2002b, a; Konopka

et al., 2012, and references therein). CLaMS results are compared with measurements from the Aura Microwave Limb Sounder (MLS). The paper is organised as follows: Sect. 2 describes the CLaMS simulations using artificial tracers. In Sect. 3, CLaMS results are presented and compared to MLS measurements. The conclusions are given in Sect. 4.

2 The Chemical Lagrangian Model of the Stratosphere (CLaMS)

2.1 Model description

Model simulations were performed using the Chemical Lagrangian Model of the Stratosphere (CLaMS), a three-dimensional chemistry transport model that was originally developed for the stratosphere (e.g. McKenna et al., 2002b, a; Grooß et al., 2005; Grooß and Müller, 2007) and extended to the troposphere (Konopka et al., 2010, 2012; Pommrich et al., 2014, and references therein). It was shown in previous studies, that CLaMS is very well-suited to simulate strong tracer gradients of chemical species in regions where transport barriers exist like the polar vortex (e.g. Günther et al., 2008; Vogel et al., 2008), the extratropical tropopause and in the vicinity of the jet streams (e.g. Pan et al., 2006; Konopka et al., 2010; Vogel et al., 2011b; Konopka and Pan, 2012).

CLaMS is based on a Lagrangian formulation of tracer transport and considers an ensemble of air parcels on a time-dependent irregular grid that is transported by use of 3-D-trajectories. The irreversible part of transport, i.e. mixing, is controlled by the local horizontal strain and vertical shear rates with mixing parameters deduced from observations (Konopka et al., 2010, and references therein). Here, we present results of global CLaMS simulations that cover an altitude range from the surface up to 900 K potential temperature (≈ 37 km altitude) with a horizontal resolution of 100 km and a maximum vertical resolution of approximately 400 m at the tropopause. The horizontal winds are taken from the ERA-Interim reanalysis (Dee et al., 2011) provided by the European Centre for Medium-Range Weather Forecasts (ECMWF). Changes are

The Asian monsoon anticyclone in summer 2012

B. Vogel et al.

Title Page

Abstract

Introduction

Conclusions

References

Tables

Figures



Back

Close

Full Screen / Esc

Printer-friendly Version

Interactive Discussion



implemented to improve deep and mid-level convection in ERA-Interim data in contrast to previous reanalysis data (Dee et al., 2011).

Mixing parameter, vertical coordinate, and the cross-isentropic velocity of the model follow the model set-up described by Konopka et al. (2012). Convection in CLaMS is represented by vertical velocities in ERA-Interim reanalysis data. CLaMS employs a hybrid coordinate (ζ), which transforms from a strictly isentropic coordinate Θ to a pressure-based coordinate system (more details see Pommrich et al., 2014).

For this study, the CLaMS simulation includes full stratospheric chemistry (Grooß et al., 2014; Sander et al., 2011) and was initialised on 1 May 2012 based on data from AURA-MLS version 3.3 (Livesey et al., 2011) and ACE-FTS version 3.0 and on results of a multi-annual CLaMS simulation started on 1 October 2001 (Konopka et al., 2010). Global O_3 , CO, H_2O , HCl, and N_2O fields are derived from MLS data within ± 2.5 days, while the trajectory-determined synoptic locations have been composed to a $2^\circ \times 6^\circ$ (latitude-longitude) grid. Below $\zeta = 350$ K (equal to $\Theta = 350$ K), these species were taken from the CLaMS multi-annual simulation with a linear transition between $\zeta = 350$ and 400 K (equal to $\Theta = 350$ –400 K). CO_2 is initialised from this simulation within the whole vertical domain.

The initialisation of CH_4 , NO_y , CFC-11, and CFC-12 was derived from N_2O using correlation fits for different latitude bins derived from ACE-FTS version 3.0 data between April and August 2010 following Grooß et al. (2014). The remaining species and the initial partitioning of the chemical families were taken from correlations and the Mainz 2-D model as described by Grooß et al. (2014). At the upper boundary (900 K potential temperature) AURA-MLS and ACE-FTS measurements and tracer-tracer correlations were used similarly as for the initialisation besides CO which was taken from MLS V3.3 data.

At the lower boundary (surface), O_3 is set to a constant tropospheric value of 4.8×10^{-8} volume mixing ratio representing the ozone mixing ratio at 5 km (Brasseur and Solomon, 2005, p. 619). Water vapour is replaced by ECMWF water vapour in lower model levels. Lower boundary conditions for CO and CH_4 are derived from AIRS

The Asian monsoon anticyclone in summer 2012

B. Vogel et al.

Title Page

Abstract

Introduction

Conclusions

References

Tables

Figures



Back

Close

Full Screen / Esc

Printer-friendly Version

Interactive Discussion



(Atmospheric Infrared Sounder) satellite measurements version 6 following the approach described by Pommrich et al. (2014).

2.1.1 Emission tracers

The aim of our study is to analyse transport pathways of air masses from boundary layer sources to the Asian monsoon anticyclone and further the transport of these air masses into the extratropical lowermost stratosphere. Three-dimensional CLaMS simulations were performed to include both the advective transport and the irreversible part of transport, namely mixing. The use of artificial tracers in CLaMS that mark particular regions in the atmosphere allows to quantify the origin of air masses, the pathways, and the transport times to be quantified (Günther et al., 2008; Vogel et al., 2011a).

Here, inert artificial tracers of air mass origin, hereafter referred to as “emission tracers”, are introduced that mark globally all land masses in the Earth’s boundary layer ($\approx 2\text{--}3\text{ km}$ above surface following orography corresponding to $\zeta < 120\text{ K}$) and thus represent regionally different boundary layer sources regions. Figure 1 shows the geographic regions defined for all 13 emission tracers (red boxes). The latitude and longitude range of each box that represents one emission tracer is listed in Table 1. Regions in the boundary layer not considered in the defined emissions tracers listed in Table 1 are summarised in an emission tracer for the background. Because we are in particular interested in the contributions of different boundary layer source regions in Asia to the composition of air within the Asian monsoon anticyclone, the regions defining emission source regions in Asia are chosen smaller than in regions elsewhere. The separation in different regions in Asia is chosen to separate regions that are currently discussed in the literature as possible source regions (see Sect. 1). The most important regions for our study are North India (NIN), South India (SIN), East China (ECH), and South-east Asia (SEA). To discuss the CLaMS results, the percentages of emission tracers for North India (NIN), South India (SIN) and East China (ECH) are sometimes summarised in one emission tracer referred to as “India/China” (India/China = NIN + SIN + ECH).

The Asian monsoon anticyclone in summer 2012

B. Vogel et al.

Title Page

Abstract

Introduction

Conclusions

References

Tables

Figures



Back

Close

Full Screen / Esc

Printer-friendly Version

Interactive Discussion



3 Results

3.1 The Asian monsoon anticyclone 2012

3.1.1 Spatio-temporal evolution of the Asian monsoon anticyclone 2012

The spatio-temporal evolution of the Asian monsoon anticyclone in summer 2012 is inferred from three-dimensional CLaMS simulations using emission tracers for Asia. The CLaMS simulation starts on 1 May 2012 before the formation of the Asian monsoon anticyclone begins during June and ends late October after the breakup of the anticyclone. Deep convection (represented in CLaMS by vertical velocities in ERA-Interim reanalysis data; see Sect. 2.1) leads to strong upward transport of emission tracers from source regions in Asia within the Asian monsoon anticyclone. Our simulation confirms that the extent, strength, and location of the anticyclone is highly variable (e.g. Annamalai and Slingo, 2001; Randel and Park, 2006; Garny and Randel, 2013). In particular, the locations of peaks with maximum contributions of emission tracers for India/China and the shape of the anticyclone change from day to day.

Because the Asian monsoon anticyclone is characterised by low PV, the horizontal distributions of the emission tracer for India/China in comparison to the horizontal distribution of PV is analysed at 380 K potential temperature (≈ 16 km) (see Figs. 2 and 3). The level of 380 K potential temperature is located within the Asian monsoon anticyclone just below the thermal tropopause (see Sect. 3.2.2). To discuss the spatio-temporal evolution of the Asian monsoon anticyclone, 6 days are selected reflecting typical situations of the evolution of the Asian monsoon anticyclone. The 1 July 2012 shows conditions at the beginning of the evolution of the Asian monsoon, here the anticyclone is centred over Tibet. The 28 July, 2 August and 8 August 2012 are days in the middle period of the monsoon season, here a strong asymmetric anticyclone, a symmetric anticyclone centred over Iran and an anticyclone split into two smaller anticyclones are found. At the end of the monsoon period on 20 September 2012, the separation of a large eastward migrating weaker anticyclone (eddy shedding event)

The Asian monsoon anticyclone in summer 2012

B. Vogel et al.

Title Page

Abstract

Introduction

Conclusions

References

Tables

Figures



Back

Close

Full Screen / Esc

Printer-friendly Version

Interactive Discussion



of the main anticyclone is found. Finally, the 19 October 2012 was selected to show the horizontal distribution of emission tracers for India/China after the breakup of the anticyclone.

On 1 July 2012 (Fig. 2, top), the anticyclone is centred over Tibet. The northern flank of the anticyclone border on the subtropical westerly jet and the southern flank to the equatorial easterly jet. In our study, the region of strongest gradients in the horizontal distribution of emission tracers from Asia represent the edge of the anticyclone at 380 K. A fixed PV value of about 4.5 PVU (thick white line) is introduced in Fig. 2 to mark regions with low PV (< 4.5 PVU). Filaments consisting of air masses characterised by low PV values (< 4.5 PVU) and enhanced emissions from India/China occur both at the western and eastern flank of the anticyclone.

On 28 July 2012 (Fig. 2, 2nd row), the horizontal distribution of high percentages of emission tracers for India/China shows an elongated structure with maxima at its two endpoints located over Northeast Africa and Southeast China (red coloured). Similar patterns are found for the absolute vorticity in theoretical calculations by Hsu and Plumb (2001) to investigate nonaxisymmetric thermally driven circulations within the monsoon dynamic. The shape of the PV isoline of 4.5 PVU includes two anticyclones situated close together.

After 28 July 2012, the western peak is transported eastwards and the eastern peak moves westwards and both peaks merge in one location in early August. On 2 August 2012 (see Fig. 2, 3rd row), the anticyclone again has a more symmetric shape and is centred over Iran and Afghanistan. The spatial distribution of emission tracers for India/China shows two regions with maximum values one in the core of the anticyclone over Iran and Afghanistan and another smaller within the anticyclone farther northeast over China. This pattern is a remnant of the elongated structure found in the distribution of emission tracers for India/China on 28 July 2012 caused by the double peak structure of the Asian monsoon anticyclone. This small-scale structure found in the horizontal distribution of emission tracers for India/China is also evident in the spatial distribution of low PV values. On 8 August 2012 (see Fig. 2, bottom), the Asian mon-

The Asian monsoon anticyclone in summer 2012

B. Vogel et al.

Title Page

Abstract

Introduction

Conclusions

References

Tables

Figures



Back

Close

Full Screen / Esc

Printer-friendly Version

Interactive Discussion



contributions from India/China within a few days (roughly 8–14 days) to the lowermost stratosphere over northern Europe. Therefore, in general filaments of smaller anticyclones separated at the northeast flank of the anticyclone have the capability to rapidly transport water vapour and pollutants from Asia to the lowermost stratosphere over North America and Europe (e.g. Vogel et al., 2014).

In 2012, the breakup of the Asian monsoon anticyclone occurred in late September and early October. Figure 3 (bottom) shows the spatial distribution of the emission tracers for India/China at 380 K after the breakup on 19 October 2012. The breakup of the anticyclone or the disappearance of the transport barrier goes along with the spread of the emission tracers for India/China at 380 K within the mid-latitudes of the Northern Hemisphere and in the tropics. High percentages of the emission tracers for India/China are found over the Pacific Ocean and over the east coast of North America along the subtropical westerly jet. The subtropical jet is in addition a transport barrier for the transport further polewards into the lowermost stratosphere of air masses originating in the boundary layer in India/China. In addition, air masses originating in the boundary layer in India/China could penetrate into the upwelling in the deep branch of the Brewer–Dobson circulation and could in this way reach the upper stratosphere.

To compare our simulation results with O_3 and CO measurements by MLS (Version 3.3) (Livesey et al., 2008), the same horizontal cross-sections as in Figs. 2 and 3 at 380 K potential temperature are shown in Figs. 4 and 5. In general at 380 K, the horizontal distributions of the stratospheric tracer O_3 show very similar patterns as the spatial distribution of the emission tracers for India/China calculated in our simulation, i.e. low ozone corresponds to high percentages of the emission tracers for India/China and vice versa. Features like the filamentary structure on the western and eastern flank of the anticyclone on 1 July 2012, the elongated double peak structure on 28 July 2012, the symmetric structure with a westward eddy shedding on 2 August 2012, the split of the anticyclone into two smaller anticyclones on 8 August 2012, the strong eastward eddy shedding event on 20 September 2012, and the tracer distribution after the breakup of the anticyclone on 19 October 2012 are also evident in the MLS O_3 mea-

The Asian monsoon anticyclone in summer 2012

B. Vogel et al.

Title Page

Abstract

Introduction

Conclusions

References

Tables

Figures



Back

Close

Full Screen / Esc

Printer-friendly Version

Interactive Discussion



The Asian monsoon anticyclone in summer 2012

B. Vogel et al.

Title Page

Abstract

Introduction

Conclusions

References

Tables

Figures



Back

Close

Full Screen / Esc

Printer-friendly Version

Interactive Discussion



surements. In addition, in the Northern Hemisphere CLaMS simulations of O_3 show the same patterns as MLS O_3 at 380 K potential temperature. Figures for CLaMS O_3 are shown in the Supplement of this paper. CO as a tropospheric tracer is expected to show high values in regions with high contributions of the emission tracers for India/China, however the features mentioned above are less distinct in MLS CO than in O_3 . Reasons for that could be deficiencies in MLS CO data (v3) in the lower stratosphere as suggested by Hegglin and Tegtmeier (2015). CLaMS CO (shown in the Supplement of this paper) shows similar pattern as MLS CO, however due to the coarse spatial resolution of MLS CO and possible deficiencies in MLS CO, the agreement is not quite as good as for O_3 . However, the comparison between CLaMS simulations and MLS measurements shows that the model yields realistic patterns of the contribution of emission tracers in the region of the Asian monsoon anticyclone at 380 K.

Previous studies (Zhang et al., 2002; Yan et al., 2011) found that the longitudinal location of the anticyclone core has two preferred regions at 100 hPa, referred to as Tibetan Mode (80–90° E) and Iranian Mode (55–65° E), impacting the spacial distribution of chemical trace gases in this region. Our simulations show that the shape of the anticyclone oscillates between a strongly symmetric anticyclone and second, a double peak structure, a strongly asymmetric anticyclone either elongated or split in two smaller anticyclones as discussed above (Figs. 2 and 3). If we assume that the highest percentages of the emission tracers for India/China are found in the core region of the anticyclone, the Tibetan Mode and Iranian Mode should be also evident in the distribution of emissions tracers for India/China in the CLaMS simulations as found for chemical constituents in the UTLS (Yan et al., 2011). Therefore, we calculate mean values of the contributions of emission tracers for India/China for July/August 2012 in latitude-longitude bins (of 2.5° longitude (λ) \times 1.0° latitude (ϕ)) at 380 K.

Figure 6 (left, top panel) shows the number of days ($N(\lambda, \phi)$) where in the region of the Asian monsoon anticyclone air masses are found with mean values of the contributions of emission tracers for India/China exceeding 35 % for July/August 2012. The value of 35 % is chosen because it considers relatively high contributions of the emis-

sion tracer for India/China. Choosing a higher percentage would not consider lower contributions of the emission tracers for India/China found in the core of the anticyclone in early July due to the transport times of air masses originating in boundary layer in India/China up to the 380 K level.

5 An accumulation of days with contributions of emission tracers for India/China larger than 35 % are found over Afghanistan/Pakistan and over Nepal/Tibet (in $\approx 1/3$ of all days in July/August) within a latitude range of 28–36° N. Maximum occurrence are found in longitude intervals of approximately 60–75 and 80–90° E (see Fig. 6 left, bottom panel). In the simulated tracer distribution, a bimodal longitudinal structure is also
10 found, however the maxima found at 60–75° E are shifted to somewhat higher longitudes compared to the Iranian Mode (55–65° E) derived by Zhang et al. (2002). Reasons could be that here the distribution of emission tracers is used in contrast to the study by Zhang et al. (2002) where the dynamical core of the anticyclone is derived based on considering geopotential on pressure surfaces of 100 hPa. It must be emphasized that this bimodal distribution has been seen in the dynamical structure of the anticyclone (Zhang et al., 2002), found in satellite measurements (Yan et al., 2011) and in the CLaMS simulations is not simply an east-west shift of the anticyclone, but rather is caused by the oscillation between strongly symmetric and asymmetric anticyclones as shown in Figs. 2 and 3 (left). Besides of the 2 maxima (modes), lower maxima are
20 found in the longitudinal distribution (see Fig. 6 left, bottom panel) at 50° E reflecting the transport of air masses from the Asian monsoon anticyclone to the west by westward eddy shedding (or outflow) and at 100° E caused by eastward eddy shedding and the release of filaments at the northeastern flank of the anticyclone (Vogel et al., 2014).

25 The same analysis is also performed for September/October 2012, the end phase of the monsoon season and its breakup (Fig. 6, right). Here, the region with an accumulation of days with contributions of emission tracers for India/China larger than 35 % (in $\approx 1/4$ of all days in September/October) is shifted to the tropics and broadened both to the east and to the west. This shows that also in September and October 2012 enhanced contributions of boundary emissions are found over Asia at 380 K, even though

The Asian monsoon anticyclone in summer 2012

B. Vogel et al.

Title Page

Abstract

Introduction

Conclusions

References

Tables

Figures



Back

Close

Full Screen / Esc

Printer-friendly Version

Interactive Discussion



the confinement of the Asian monsoon anticyclone has dissipated during that time period. Also here, a bimodal distribution is found with two maxima one at 40–60° E and a second at 75–110° E (Fig. 6 right, bottom panel).

Animations showing the temporal evolution (on a daily basis) of the contribution of emission tracers for India/China and PV at 380 K potential temperature on the Northern Hemisphere during the Asian monsoon season 2012 (1 May 2012–late October 2012) are available as a Supplement of this paper showing the intraseasonal variability of the Asian monsoon anticyclone. In the next section, the spatial distribution of different emission tracers for Asia within the Asian monsoon anticyclone and the temporal evolution of all tracers within the Asian monsoon anticyclone from May until late October 2012 are discussed.

3.1.2 Impact of different emission tracers to the composition of the Asian monsoon anticyclone

To analyse the possible impact of different boundary layer source regions in Asia, in particular the specific importance of Southeast Asia, to the composition of the Asian monsoon anticyclone, the horizontal distributions of emission tracers are discussed at 380 K potential temperature using the four days introduced in the previous section (1 July, 2 and 8 August, and 20 September 2012, see Sect. 3.1.1). The emission tracers for North India, South India, and East China show in principle the same horizontal patterns, therefore here we show only emissions from North India. However their individual contributions to the composition of the anticyclone differ from tracer to tracer (see Sect. 3.1.3). It turns out that the spatial distribution of the emission tracer for Southeast Asia has a fundamentally different behaviour than the distribution for emission tracers for North India, South India, and East China at 380 K potential temperature.

Figure 7 shows the horizontal distribution of emission tracers for North India (NIN) (left) and Southeast Asia (SEA) (right) at 380 K potential temperature over Asia on 1 July 2012 (top), 2 August 2012 (2nd row), 8 August 2012 (3rd row), and 20 September (bottom). On 1 July 2012 (Fig. 7, top), air masses from boundary layer sources in North

The Asian monsoon anticyclone in summer 2012

B. Vogel et al.

Title Page

Abstract

Introduction

Conclusions

References

Tables

Figures



Back

Close

Full Screen / Esc

Printer-friendly Version

Interactive Discussion



The Asian monsoon anticyclone in summer 2012

B. Vogel et al.

Title Page

Abstract

Introduction

Conclusions

References

Tables

Figures



Back

Close

Full Screen / Esc

Printer-friendly Version

Interactive Discussion



India and Southeast Asia are confined within the Asian monsoon anticyclone and within the filaments at its western and eastern flank. Air masses influenced by boundary layer sources from Southeast Asia are in addition found in the tropics. Within the anticyclone the emission tracer for Southeast Asia has the largest contribution at 380 K, followed by the emission tracers for North India. The contributions of the emissions tracer for South India is in the same order of magnitude as for North India and the lowest fraction is found for the emission tracer for East China (not shown here).

Similar as for 1 July 2012, on 2 August 2012 at 380 K (Fig. 7, 2nd row, left) the distribution of the emission tracer for North India is also confined within the Asian monsoon anticyclone. Filaments containing enhanced contributions of the emission tracer for North India exist also at the western and eastern flank of the anticyclone. Contrary to the 1 July at the beginning of August, the highest percentages of emission tracers within the anticyclone are from North India and East China (not shown here), thus the impact of boundary sources located more northwards is larger than the impact of boundary sources from Southeast Asia and South India (not shown here).

Further on 2 August 2012 at 380 K, the spatial distribution of the emission tracers for North India shows two regions with maximum values, one in the core of the anticyclone over Iran and Afghanistan and another within the anticyclone farther northeast over China which is a remnant of a double peak structure found on 28 July 2012 as discussed above in Sect. 3.1.1.

In contrast to the 1 July, on 2 August 2012 (Fig. 7, 2nd row, right) enhanced percentages of the emission tracer for Southeast Asia are found at the edge of the anticyclone in particular at the southeast edge of the anticyclone and in the western and eastern filaments of the anticyclone. Further looking at a wider geographical scale, large contributions of the emission tracer for Southeast Asia are found south of the anticyclone in the tropics, over the Pacific Ocean and west of the anticyclone over the South Atlantic Ocean. Low percentages of the emission tracer for Southeast Asia are found in the core of the anticyclone in contrast to the emission tracer for North India (and East China, not shown here) having large contributions in the core. The spatial distribution

of the emission tracer for Southeast Asia within the anticyclone is like a negative image to the spatial distribution of the emission tracer for North India.

On 8 August 2012 (Fig. 7, 3rd row), the Asian monsoon anticyclone is split into two smaller anticyclones. Apart from the double peak structure, the spatial distribution of the emission tracer for North India and Southeast Asia is similar to the distribution on 2 August 2012. Remarkable are high percentages of the emission tracer for Southeast Asia at the edge of the two anticyclones and low percentages inside the two anticyclones. Thus at the beginning of August 2012, the percentage of emission tracers for North India and East China (not shown here) outweigh the percentage of the emission tracers from further south for Southeast Asia and South India (not shown) inside the anticyclone in contrast to the conditions in early July.

Air masses originating in Southeast Asia can experience strong uplift by deep convection (e.g. Park et al., 2007; Li et al., 2005) or typhoons (Vogel et al., 2014). If an air parcel is uplifted at the edge of the Asian monsoon to altitudes high enough, it can be entrained into the anticyclonic circulation and subsequent clockwise transport of the air parcel around the outer edge of the anticyclone occurs. The edge of the anticyclone acts here as a strong transport barrier evident in the strong gradients of the different emission tracers at the edge of the anticyclone (more details see Sect. 3.2.2). The transport barrier acts in both directions, namely for inward transport apparent in the tracer distribution from Southeast Asia and for outward transport apparent in the tracer distribution for North India (see Fig. 7, 2nd and 3rd row). Further, air masses originating in the boundary layer in Southeast Asia are uplifted in the tropics at locations where they do not reach the Asian monsoon anticyclone. A subsequently isentropic poleward transport of these air masses from the tropics to the region of the Asian monsoon anticyclone is evident in the CLaMS simulation (see Sect. 3.2.1).

On 20 September 2012 (see Fig. 7, bottom), the anticyclone is shifted to the south compared to the location of the Asian monsoon anticyclone in July and August. In the core of the Asian monsoon anticyclone, the main contributions are emission tracers for Southeast Asia and North India followed by East China (not shown). A smaller

The Asian monsoon anticyclone in summer 2012

B. Vogel et al.

Title Page

Abstract

Introduction

Conclusions

References

Tables

Figures



Back

Close

Full Screen / Esc

Printer-friendly Version

Interactive Discussion



percentage is found for the emission tracer for South India (not shown). Further, on 20 September 2012 (see Fig. 7, bottom), a strong eastward eddy shedding event occurred as discussed in the previous Sect. 3.1.1. In general during an eastward eddy shedding event, air masses from the core of the anticyclone can be mixed with air masses from the edge of the Asian monsoon anticyclone. Air masses separated in the second smaller anticyclone is transported eastwards by the subtropical jet to North America and Europe as discussed in Vogel et al. (2014).

Further, on 20 September 2012 at the end of the monsoon season, the spatial distribution of the emission tracer for Southeast Asia at 380 K is very different compared to the distributions of the emission tracer for North India in particular within the Northern Hemisphere. During the end of the monsoon season, contributions of the emission tracers for North India are still trapped within the anticyclone. As discussed before, air masses originating in the boundary layer in Southeast Asia are uplifted both within the Asian monsoon anticyclone and elsewhere in the tropics. Uplift in the tropics and subsequent isentropic poleward transport at around 380 K yield propagation of air masses originating in the boundary layer of Southeast Asia to mid-latitudes (more details are discussed below in Sect. 3.2.1). Therefore, high percentages of the emission tracer for Southeast Asia is more widely distributed compared to emission tracers for North India, South India and East China. A movie showing the temporal evolution (on a daily basis) of the contribution of emission tracers for Southeast Asia at 380 K potential temperature on the Northern Hemisphere during the Asian monsoon 2012 (1 May 2012–late October 2012) is available as a Supplement of this paper.

3.1.3 Temporal evolution of different emission tracers

After presenting the spatial distribution of the emission tracers for four selected days, we discuss the temporal evolution of different emission tracers within the Asian monsoon anticyclone in 2012. In the previous sections, it is shown that the area enclosed by the 4.5 PVU isoline constitutes a good upper boundary for the area within the Asian monsoon anticyclone at 380 K showing enhanced contributions of emission tracers

The Asian monsoon anticyclone in summer 2012

B. Vogel et al.

Title Page

Abstract

Introduction

Conclusions

References

Tables

Figures



Back

Close

Full Screen / Esc

Printer-friendly Version

Interactive Discussion



for India/China within the Asian monsoon anticyclone. Ploeger et al. (2015) inferred a mean value of 3.8 PVU to mark the transport barrier for the Asian monsoon anticyclone 2012 at 380 K using the PV gradient and horizontal circulation. However, the PV value marking the transport barrier changes from day to day with maximum PV values up to 4.4–4.6 PVU and could only be deduced for a period from 20 June to 20 August 2012 (Ploeger et al., 2015). In this study, a value of 4.5 PVU is used which is in agreement with the upper limit of the PV values derived by Ploeger et al. (2015) and is extrapolated to early June and September/October 2012.

Therefore, to calculate the percentage of different emission tracers within the Asian monsoon anticyclone at 380 K, we use the following assumption. Mean values of all emission tracers are calculated in Asia for the region between 15 and 50° N and 0 and 140° E (at 380 ± 0.5 K, shown as black box in Fig. 7). In addition to this geographical limit (black box), PV values lower than 4.5 PVU are required to calculate the mean values of the different emission tracers within the Asian monsoon anticyclone for each day as shown in Fig. 8.

The contribution of different emission tracers from Asia within the anticyclone differ in time and from tracer to tracer (Fig. 8). The temporal evolution shows that contributions of the emission tracer for Southeast Asia (black) are found within the Asian monsoon anticyclone at 380 K potential temperature end of May that is roughly 2 weeks before contributions of the emission tracers for North India (red), South India (blue), and East China (green) reach at that level of potential temperature. At the beginning of the Asian monsoon period in June/early July, contributions of air masses originating in South Asia dominate within the anticyclone with maximum percentages of emission tracers on average of 13 % for Southeast Asia (black) and 6.5 % for South India (blue) at 380 K. During July 2012, the contributions of emission tracers for the south decrease to 10 % (Southeast Asia) and 6 % (South India) and contributions of emission tracers for the north, for North India (red) and East China (green) increase up to 18 and 10 %, respectively, until early August. During August 2012, the percentage of the emission tracers for the south rise again until the breakup of the anticyclone which

The Asian monsoon anticyclone in summer 2012

B. Vogel et al.

[Title Page](#)[Abstract](#)[Introduction](#)[Conclusions](#)[References](#)[Tables](#)[Figures](#)[Back](#)[Close](#)[Full Screen / Esc](#)[Printer-friendly Version](#)[Interactive Discussion](#)

The Asian monsoon anticyclone in summer 2012

B. Vogel et al.

Title Page

Abstract

Introduction

Conclusions

References

Tables

Figures



Back

Close

Full Screen / Esc

Printer-friendly Version

Interactive Discussion



occurred end of September in contrast to decreasing contributions of emission tracers for North India. Our simulations show that a south-north shift in the contribution of different emission tracers for Asia within the Asian monsoon anticyclone occurred during the summer 2012 possibly linked to the northward moving long-term intraseasonal variations (30 to 60 day oscillations) found in monsoon activity like rainfall (e.g. Goswami, 2012, and references therein).

During August and September 2012, contributions of the emission tracer for North India (red) decrease in principle, but show local maxima end of August and end of September. In the same time period, contributions of the emission tracer for East China show a slight increase with maximum percentages end of September. Thus in our simulations, an oscillation with a period of roughly 10–20 days is found in the contributions of the emission tracer for North India during August and September. We suggest that these oscillations are most likely connected to the short-term westward propagating intraseasonal variations (10–20 days) of the Asian summer monsoon found on a smaller horizontal scale (e.g. Goswami, 2012, and references therein).

At the end of September 2012, the contributions of emission tracers for North India, South India, and East China start to decrease caused by the breakup of the Asian monsoon anticyclone and the missing upward transport within the anticyclone. In contrast to these tracers, the contribution of emission tracers for Southeast Asia increases continuously up to 23 % from its minimum percentage of 10 % in late August until end of October. In early October, the anticyclone had already dissolved, however the contributions of the emission tracer for Southeast Asia still rise. The reason for this increase is that air masses originating in the boundary layer in Southeast Asia experienced in addition to the upward transport in the Asian monsoon anticyclone itself, uplift in the tropics and rapid uplift over the Pacific Ocean. The contribution of the emission tracer for the background (grey line in Fig. 8, see Sect. 2.1.1) also shows a strong increase after the breakup of the anticyclone indicating an uplift of air masses outside of Asia. The influence of other land masses (yellow line in Fig. 8) is of minor importance throughout the considered time period. Note that the sum of all emission tracers shown in Fig. 8 is

North India (NIN), South India (SIN), and East China (ECH)) are confined within the anticyclone similar to 380 K potential temperature, however the percentages are higher at 360 and lower at 400 K (see Fig. 9). Highest percentages of the emission tracer for India/China are found in the core of the anticyclone, indicating a slow upward transport of emissions from India/China within the Asian monsoon anticyclone.

The distribution of the emission tracer for Southeast Asia (see Fig. 10) within the anticyclone is different compared to the distribution of the emission tracers for India/China (see Fig. 9). In addition to the convectively driven uplift within the Asian monsoon, air masses from Southeast Asia experience further upward transport pathways. First, strong convective uplift occurred in the Pacific (Li et al., 2005) e.g. caused by typhoons (Vogel et al., 2014) at the southeast flank of the Asian monsoon anticyclone. Afterwards these emissions can be entrained into the outer circulation of the Asian monsoon anticyclone and are transported clockwise at the edge of the circulation around the core of the Asian monsoon anticyclone. Therefore in general, a high percentage of the emission tracer for Southeast Asia is found at the edge of the Asian monsoon anticyclone as evident at 360 K (see Fig. 10, left). This finding is consistent with backward trajectory calculations by Vogel et al. (2014) for the same time period, that show that air masses originating in Southeast Asia circulate in an upward spiral around the core of the Asian monsoon anticyclone. In contrast, at 400 K potential temperature, high percentages of air masses originating in Southeast Asia are found within the anticyclone similar as for the emission tracer for India/China and lower contributions of the emission tracer for Southeast Asia are found outside the anticyclone. This indicates an upward transport of air masses from Southeast Asia at the edge of the anticyclone up to the top of the anticyclone at around 400 K in contrast to the upward transport of air masses from India/China within the core of the anticyclone.

A second upward transport pathways for the emission tracer for Southeast Asia is uplift of in the deep tropics. Its impact on the chemical composition of lowermost stratosphere is discussed in the next Sect. 3.2.1.

The Asian monsoon anticyclone in summer 2012

B. Vogel et al.

Title Page

Abstract

Introduction

Conclusions

References

Tables

Figures



Back

Close

Full Screen / Esc

Printer-friendly Version

Interactive Discussion



The Asian monsoon anticyclone in summer 2012

B. Vogel et al.

Title Page

Abstract

Introduction

Conclusions

References

Tables

Figures



Back

Close

Full Screen / Esc

Printer-friendly Version

Interactive Discussion



level the isentropic transport from the tropics to higher latitudes is weaker than below at the level of 380 K potential temperature. As a result, the Northern and Southern Hemisphere are flooded around 380 K with air masses originating in the boundary layer of Southeast Asia, that means that air masses are younger in September than before the Asian monsoon season at that level of potential temperature. Thus in the Northern Hemisphere, air masses from Southeast Asia are uplifted in the tropics and are widely distributed around the anticyclone caused by the anticyclonic flow in this region acting as a large stirrer. The subtropical jets in both hemispheres act as transport barrier for transport from the upper troposphere into the lowermost stratosphere. This quasi-horizontal transport of air masses from the tropical tropopause layer (TTL) to higher latitudes yields moistening of the extratropical lowermost stratosphere (e.g. Ploeger et al., 2013; Spang et al., 2015).

Moreover, air masses from the the Asian monsoon anticyclone including air masses originating in Southeast Asia and also from India/China can be separated from the main circulation at its northern flank by eastward eddy shedding or release of filaments. These wet and polluted air masses are transported eastwards along the subtropical jets (e.g. Vogel et al., 2014) and can be transported most likely by Rossby wave breaking into the lowermost stratosphere. Afterwards, enhanced contributions of emission tracers for Asia are found in the extratropical lowermost stratosphere.

After the breakup of the Asian monsoon anticyclone in October 2012, also air masses with contributions from boundary emission from North India, South India, and East China that were trapped before within the anticyclone are distributed globally within the lowermost stratosphere (see Fig. 3, bottom left, and animations in the Supplement of this paper).

3.2.2 Gateways for air masses from the anticyclone to the stratosphere

Possible vertical transport at the top of the Asian monsoon anticyclone around the tropopause and possible isentropic transport at the edge of the anticyclonic circulation is discussed analysing the spatial distribution of emission tracers for Asia in CLaMS.

The Asian monsoon anticyclone in summer 2012

B. Vogel et al.

Title Page

Abstract

Introduction

Conclusions

References

Tables

Figures



Back

Close

Full Screen / Esc

Printer-friendly Version

Interactive Discussion



We have chosen the 20 September 2012 as an example, already shown in Figs. 3 (top) and 7 (bottom). Figure 11 shows latitude-height cross-sections across the area of the Asian Monsoon anticyclone at 80° E longitude of (a) static stability (buoyancy frequency squared, N^2), the contributions of the emission tracers for (b) India/China (= North India (NIN) + South India (SIN) + East China (ECH); see Sect. 2.1.1), (c) Southeast Asia (SEA), and (d) Siberia (SIB) on 20 September 2012. Figure 11a shows that the thermal tropopause (black dots) above the anticyclone ($\approx 15\text{--}35^\circ\text{N}$) is elevated (e.g. Dunkerton, 1995; Highwood and Hoskins, 1998). The anticyclone is flanked by the subtropical westerly jet in the north ($\approx 30\text{--}40^\circ\text{N}$) and the equatorial easterly jet in the south ($\approx 0\text{--}10^\circ\text{N}$) (wind velocities of both jets are shown as black lines). Further at its northern flank, a double thermal tropopause (at ≈ 340 and 400 K potential temperature) is found between 40 and 60° N. Multiple tropopauses occur often at the northern flank of the Asian monsoon anticyclone along the subtropical jet (e.g. Manney et al., 2014). The potential temperature level at 380 K is marked as a purple line to illustrate the position of the horizontal cross-sections shown in Figs. 3 (top) and 7 (bottom). The 380 K level is just below the thermal tropopause (black dots) in the tropics and within the Asian monsoon anticyclone, however north of the anticyclone it is above the first tropopause and therefore within the lowermost stratosphere. In general, tropospheric air masses, including air masses within the Asian monsoon anticyclone, are characterised by low values of N^2 in contrast to stratospheric air masses. High values (dark red) of N^2 found directly above the first tropopause characterise the tropopause inversion layer (TIL) (e.g. Birner et al., 2006). Figure 11a shows that sandwiched between the double tropopause at the northern flank of the anticyclone low values of N^2 (shown in blue/green) occur in comparison to the stratospheric background on 20 September 2012 indicating that tropospheric air masses from the Asian monsoon anticyclone was isentropically transported into the lowermost stratosphere.

Figure 11b shows that high percentages of the emission tracers for India/China are transported upward within the Asian monsoon anticyclone up to the thermal tropopause and are trapped within the anticyclone ($\approx 15\text{--}35^\circ\text{N}$). Enhanced contributions of the

emissions tracers for India/China are in addition found on the Southern Hemisphere on the equatorial flank of the subtropical jet, indicating additional upward transport elsewhere in the tropics.

In contrast, air masses originating in the boundary layer in Southeast Asia (see Fig. 11c) are released at latitudes lower (12° S– 20° N) than air masses originating in India/China (0 – 40° N) therefore air masses from Southeast Asia are uplifted both within the Asian monsoon anticyclone and elsewhere in the tropics. High percentages of the emission tracer for Southeast Asia are found up to $\approx 50\%$ at southern edge of the anticyclone, up to $\approx 20\%$ within the anticyclone, and up to ≈ 25 – 30% elsewhere in the tropics. Figure 11c shows that the upward transport of air masses originating in Southeast Asia within the Asian monsoon anticyclone can not be isolated from the transport in the deep tropics as also reported by Gettelman et al. (2004) and Bannister et al. (2004).

Further, Fig. 11b and c shows that the thermal tropopause acts as a transport barrier for emission tracers for India/China and Southeast Asia. Only a very shallow mixing layer is found around the tropopause above the anticyclone (≈ 15 – 35° N). Therefore the tropopause constitutes an upper boundary of the Asian monsoon anticyclone as expected from satellite measurements of tropospheric trace gases (see Sect. 1). In the deep tropics (≈ 10 – 25° S), enhanced percentages of the emission tracer for India/China and Southeast Asia are found above the tropopause (≈ 380 K) in late September, indicating a possible vertical upward transport into the stratosphere over the course of 5 months of CLaMS simulation.

Figure 11b and c shows enhanced contributions of emission tracers for both India/China and Southeast Asia north of the Asian monsoon anticyclone between the double tropopause and further to the north at higher latitudes indicating an isentropic transport of trace gases from the anticyclone into the lowermost stratosphere as already indicated by N^2 (see Fig. 11a). In contrast, contributions of the emission tracer for Siberia (see Fig. 11d) are not found in the lowermost stratosphere confirming that in mid- and high latitudes the first troposphere acts as a transport barrier and that vertical

The Asian monsoon anticyclone in summer 2012

B. Vogel et al.

Title Page

Abstract

Introduction

Conclusions

References

Tables

Figures



Back

Close

Full Screen / Esc

Printer-friendly Version

Interactive Discussion



of the Asian monsoon anticyclone show strong intraseasonal variations. Therefore the processes are more complex than hitherto believed.

In addition, emissions from Southeast Asia are found both within the Asian monsoon anticyclone and at the outer edge of the anticyclone. CLaMS simulations show that emissions from Southeast Asia can be rapidly uplifted by deep convection (Li et al., 2005; Chen et al., 2012) or typhoons (Vogel et al., 2014) up to the outer edge of the anticyclone (at around 380 K). Afterwards, the emissions are entrained by the anticyclonic circulation of the Asian monsoon and circulate clockwise, in an upward spiral, at the edge of the Asian monsoon anticyclone around its core (this is also true if the anticyclone is split into two smaller anticyclones).

Further, our simulations confirm that the thermal tropopause above the anticyclone constitutes a vertical transport barrier, as expected from satellite observations (e.g. Rosenlof et al., 1997; Jackson et al., 1998; Park et al., 2004, 2008; Li et al., 2005; Xiong et al., 2009). Upward transport of air masses from India/China or Southeast Asia into the lower stratosphere can occur in the deep tropics by entrainment into the upward Brewer–Dobson circulation, however the time scales to reach altitudes much higher than 400 K potential temperature are longer than one monsoon season. Furthermore, in our simulations enhanced contributions of emission tracers for India/China and Southeast Asia are found at the northern flank of the Asian monsoon anticyclone between double tropopauses indicating an isentropic transport from the anticyclone into the lowermost stratosphere.

Moreover, our simulation shows that air masses originating in Southeast Asia can be uplifted elsewhere in the deep tropics and subsequently spread out during the simulation globally on the tropical side of the subtropical jet streams in both hemispheres at around 380 K, in contrast to emissions from North India, South India, and East China that are trapped in the Asian monsoon anticyclone. During the summer 2012, this mechanism caused flooding of the lowermost stratosphere with relatively young air masses carrying moisture and pollution from Southeast Asia. Finally, after the breakup of the Asian monsoon anticyclone in October 2012, also emissions from

The Asian monsoon anticyclone in summer 2012

B. Vogel et al.

Title Page

Abstract

Introduction

Conclusions

References

Tables

Figures



Back

Close

Full Screen / Esc

Printer-friendly Version

Interactive Discussion



North India, South India, and East China that were trapped before within the Asian monsoon anticyclone were distributed globally within the UTLS.

Our findings demonstrate that emissions from India/China and Southeast Asia affected by the circulation of the Asian monsoon anticyclone have a significant impact on the chemical compositions of the lowermost stratosphere of the Northern Hemisphere in particular at end of the monsoon season in September/October 2012. The resulting moistening of the the lowermost stratosphere has a potential impact on surface climate (e.g. Solomon et al., 2010; Riese et al., 2012).

**The Supplement related to this article is available online at
doi:10.5194/acpd-15-9941-2015-supplement.**

Acknowledgements. The authors sincerely thank Paul Konopka, Felix Plöger, and Reinhold Spang (all at Research Centre Jülich) for helpful discussions. We thank the MLS scientific team (Aura Microwave Limb Sounder) for providing satellite data and the European Centre of Medium-Range Weather Forecasts (ECMWF) for providing the ERA-Interim reanalysis data. The authors gratefully acknowledge the computing time granted on the supercomputer JU-ROPA at Jülich Supercomputing Centre (JSC) under the VSR project ID JICG11. Our activities were partly funded by the German Science Foundation (Deutsche Forschungsgemeinschaft, DFG) under the DFG project LASSO (HALO-SPP 1294/GR 3786). This work also supports the campaign activities within the StratoClim project founded by the European Commission (under grant number StratoClim-603557-FP7-ENV.2013.6.1-2).

The article processing charges for this open-access publication were covered by a Research Centre of the Helmholtz Association.

References

Annamalai, H. and Slingo, J. M.: Active/break cycles: diagnosis of the intraseasonal variability of the Asian Summer Monsoon, *Clim. Dynam.*, 18, 85–102, 2001. 9949

The Asian monsoon anticyclone in summer 2012

B. Vogel et al.

Title Page

Abstract

Introduction

Conclusions

References

Tables

Figures



Back

Close

Full Screen / Esc

Printer-friendly Version

Interactive Discussion



The Asian monsoon anticyclone in summer 2012

B. Vogel et al.

Title Page

Abstract

Introduction

Conclusions

References

Tables

Figures



Back

Close

Full Screen / Esc

Printer-friendly Version

Interactive Discussion



- Bannister, R. N., O'Neill, A., Gregory, A. R., and Nissen, K. M.: The role of the south-east Asian monsoon and other seasonal features in creating the “tape-recorder” signal in the Unified Model, *Q. J. Roy. Meteor. Soc.*, 130, 1531–1554, 2004. 9944, 9966
- Bergman, J. W., Fierli, F., Jensen, E. J., Honomichl, S., and Pan, L. L.: Boundary layer sources for the Asian anticyclone: regional contributions to a vertical conduit, *J. Geophys. Res.*, 118, 2560–2575, doi:10.1002/jgrd.50142, 2013. 9944, 9968
- Bian, J., Pan, L. L., Paulik, L., Vömel, H., and Chen, H.: In situ water vapor and ozone measurements in Lhasa and Kunmin during the Asian summer monsoon, *Geophys. Res. Lett.*, 39, L19808, doi:10.1029/2012GL052996, 2012. 9943
- Birner, T., Sankey, D., and Shepherd, T. G.: The tropopause inversion layer in models and analyses, *Geophys. Res. Lett.*, 33, L14804, doi:10.1029/2006GL026549, 2006. 9965
- Bourassa, A. E., Robock, A., Randel, W. J., Deshler, T., Rieger, L. A., Lloyd, N. D., Llewellyn, E. J. T., and Degenstein, D. A.: Large volcanic aerosol load in the stratosphere linked to Asian monsoon transport, *Science*, 337, 78–81, doi:10.1126/science.1219371, 2012. 9943
- Brasseur, G. and Solomon, S.: *Aeronomy of the Middle Atmosphere: Chemistry and Physics of the Stratosphere and Mesosphere*, 3rd edn., Springer, Heidelberg, Germany, 2005. 9947
- Chen, B., Xu, X. D., Yang, S., and Zhao, T. L.: Climatological perspectives of air transport from atmospheric boundary layer to tropopause layer over Asian monsoon regions during boreal summer inferred from Lagrangian approach, *Atmos. Chem. Phys.*, 12, 5827–5839, doi:10.5194/acp-12-5827-2012, 2012. 9944, 9968, 9969
- Dee, D. P., Uppala, S. M., Simmons, A. J., Berrisford, P., Poli, P., Kobayashi, S., Andrae, U., Balmaseda, M. A., Balsamo, G., Bauer, P., Bechtold, P., Beljaars, A. C. M., van de Berg, L., Bidlot, J., Bormann, N., Delsol, C., Dragani, R., Fuentes, M., Geer, A. J., Haimberger, L., Healy, S. B., Hersbach, H., Holm, E. V., Isaksen, I., Kallberg, P., Koehler, M., Matricardi, M., McNally, A. P., Monge-Sanz, B. M., Morcrette, J.-J., Park, B.-K., Peubey, C., de Rosnay, P., Tavolato, C., Thepaut, J.-N., and Vitart, F.: The ERA-Interim reanalysis: configuration and performance of the data assimilation system, *Q. J. Roy. Meteor. Soc.*, 137, 553–597, doi:10.1002/qj.828, 2011. 9946, 9947
- Dethof, A., O'Neill, A., Slingo, J. M., and Smit, H. G. J.: A mechanism for moistening the lower stratosphere involving the Asian summer monsoon, *Q. J. Roy. Meteor. Soc.*, 556, 1079–1106, 1999. 9943

The Asian monsoon anticyclone in summer 2012

B. Vogel et al.

Title Page

Abstract

Introduction

Conclusions

References

Tables

Figures



Back

Close

Full Screen / Esc

Printer-friendly Version

Interactive Discussion



- Dunkerton, T. J.: Evidence of meridional motion in the summer lower stratosphere adjacent to monsoon regions, *J. Geophys. Res.*, 100, 16675–16688, 1995. 9965
- Dvortsov, V. L. and Solomon, S.: Response of the stratospheric temperatures and ozone to past and future increases in stratospheric humidity, *J. Geophys. Res.*, 106, 7505–7514, 2001. 9944
- 5 Fadnavis, S., Semeniuk, K., Pozzoli, L., Schultz, M. G., Ghude, S. D., Das, S., and Kakatkar, R.: Transport of aerosols into the UTLS and their impact on the Asian monsoon region as seen in a global model simulation, *Atmos. Chem. Phys.*, 13, 8771–8786, doi:10.5194/acp-13-8771-2013, 2013. 9943
- 10 Fadnavis, S., Schultz, M. G., Semeniuk, K., Mahajan, A. S., Pozzoli, L., Sonbawne, S., Ghude, S. D., Kiefer, M., and Eckert, E.: Trends in peroxyacetyl nitrate (PAN) in the upper troposphere and lower stratosphere over southern Asia during the summer monsoon season: regional impacts, *Atmos. Chem. Phys.*, 14, 12725–12743, doi:10.5194/acp-14-12725-2014, 2014. 9943, 9944
- 15 Fairlie, T. D., Vernier, J.-P., Natarajan, M., and Bedka, K. M.: Dispersion of the Nabro volcanic plume and its relation to the Asian summer monsoon, *Atmos. Chem. Phys.*, 14, 7045–7057, doi:10.5194/acp-14-7045-2014, 2014. 9943
- Forster, P. and Shine, K. P.: Stratospheric water vapour change as possible contributor to observed stratospheric cooling, *Geophys. Res. Lett.*, 26, 3309–3312, doi:10.1029/1999GL010487, 1999. 9943
- 20 Forster, P. and Shine, K. P.: Assessing the climate impact of trends in stratospheric water vapor, *Geophys. Res. Lett.*, 29, 10-1–10-4, doi:10.1029/2001GL013909, 2002. 9943
- Fromm, M., Kablick III, G., Nedoluha, G., Carboni, E., Grainger, R., Campbell, J., and Lewis, J.: Correcting the record of volcanic stratospheric aerosol impact: Nabro and Sarychev Peak, *J. Geophys. Res.*, 119, 10343–10364, doi:10.1002/2014JD021507, 2014. 9943
- 25 Garny, H. and Randel, W. J.: Dynamic variability of the Asian monsoon anticyclone observed in potential vorticity and correlations with tracer distributions, *J. Geophys. Res.*, 118, 13421–13433, doi:10.1002/2013JD020908, 2013. 9945, 9949
- Gettelman, A., Kinnison, D., Dunkerton, T. J., and Brasseur, G. P.: Impact of monsoon circulations on the upper troposphere and lower stratosphere, *J. Geophys. Res.*, 109, D22101, doi:10.1029/2004JD004878, 2004. 9944, 9966
- 30

The Asian monsoon anticyclone in summer 2012

B. Vogel et al.

Title Page

Abstract

Introduction

Conclusions

References

Tables

Figures



Back

Close

Full Screen / Esc

Printer-friendly Version

Interactive Discussion



- Goswami, B. N.: South Asian monsoon, in: *Intraseasonal Variability in the Atmosphere-Ocean Climate System*, 2nd edn., chap. 2, edited by: Lau, W. K. M. and Waliser, D. E., Springer-Verlag, Berlin, Heidelberg, 21–72, 2012. 9945, 9951, 9960, 9968
- Grooß, J.-U. and Müller, R.: Simulation of ozone loss in Arctic winter 2004/2005, *Geophys. Res. Lett.*, 34, L05804, doi:10.1029/2006GL028901, 2007. 9946
- Grooß, J.-U., Konopka, P., and Müller, R.: Ozone chemistry during the 2002 Antarctic vortex split, *J. Atmos. Sci.*, 62, 860–870, 2005. 9946
- Grooß, J.-U., Engel, I., Borrmann, S., Frey, W., Günther, G., Hoyle, C. R., Kivi, R., Luo, B. P., Molleker, S., Peter, T., Pitts, M. C., Schlager, H., Stiller, G., Vömel, H., Walker, K. A., and Müller, R.: Nitric acid trihydrate nucleation and denitrification in the Arctic stratosphere, *Atmos. Chem. Phys.*, 14, 1055–1073, doi:10.5194/acp-14-1055-2014, 2014. 9947
- Günther, G., Müller, R., von Hobe, M., Stroh, F., Konopka, P., and Volk, C. M.: Quantification of transport across the boundary of the lower stratospheric vortex during Arctic winter 2002/2003, *Atmos. Chem. Phys.*, 8, 3655–3670, doi:10.5194/acp-8-3655-2008, 2008. 9946, 9948
- Hegglin, M. I., and Tegtmeier, S. (Eds.): *SPARC Data Initiative: Assessment of Stratospheric Trace Gas and Aerosol Climatologies from Satellite Limb Sounders*, SPARC Report No. 7, in preparation, 2015. 9953
- Highwood, E. J. and Hoskins, B. J.: The tropical tropopause, *Q. J. Roy. Meteor. Soc.*, 124, 1579–1604, 1998. 9965
- Holton, J. R., Haynes, P., McIntyre, M. E., Douglass, A. R., Rood, R. B., and Pfister, L.: Stratosphere-troposphere exchange, *Rev. Geophys.*, 33, 403–439, 1995.
- Hsu, C. J. and Plumb, R. A.: Nonaxisymmetric thermally driven circulations and upper-tropospheric monsoon dynamics, *J. Atmos. Sci.*, 57, 1255–1276, 2001. 9945, 9950
- Jackson, D. R., Driscoll, S. J., Highwood, E. J., Harries, J. E., and Russell III, J. M.: Troposphere to stratosphere transport at low latitudes as studies using HALOE observations of water vapor 1992–1997, *Q. J. Roy. Meteor. Soc.*, 124, 169–192, 1998. 9943, 9969
- Kirk-Davidoff, D. B., Hints, E. J., Anderson, J. G., and Keith, D. W.: The effect of climate change on ozone depletion through changes in stratospheric water vapour, *Nature*, 402, 399–401, doi:10.1038/46521, 1999. 9944
- Konopka, P. and Pan, L. L.: On the mixing-driven formation of the Extratropical Transition Layer (ExTL), *J. Geophys. Res.*, 117, D18301, doi:10.1029/2012JD017876, 2012. 9946

The Asian monsoon anticyclone in summer 2012

B. Vogel et al.

Title Page

Abstract

Introduction

Conclusions

References

Tables

Figures



Back

Close

Full Screen / Esc

Printer-friendly Version

Interactive Discussion



- Konopka, P., Grooß, J.-U., Günther, G., Ploeger, F., Pommrich, R., Müller, R., and Livesey, N.: Annual cycle of ozone at and above the tropical tropopause: observations versus simulations with the Chemical Lagrangian Model of the Stratosphere (CLaMS), *Atmos. Chem. Phys.*, 10, 121–132, doi:10.5194/acp-10-121-2010, 2010. 9943, 9946, 9947
- 5 Konopka, P., Ploeger, F., and Müller, R.: Entropy- and static stability-based Lagrangian model grids, in: *Geophysical Monograph Series: Lagrangian Modeling of the Atmosphere*, vol. 200, edited by: Lin, J., American Geophysical Union, 99–109, doi:10.1029/2012GM001253, 2012. 9945, 9946, 9947
- Li, Q., Jiang, J. H., Wu, D. L., Read, W. G., Livesey, N. J., Waters, J. W., Zhang, Y., Wang, B., Filipiak, M. J., Davis, C. P., Turquety, S., Wu, S., Park, R. J., Yantosca, R. M., and Jacob, D. J.: Convective outflow of South Asian pollution: a global CTM simulation compared with EOS MLS observations, *Geophys. Res. Lett.*, 32, L14826, doi:10.1029/2005GL022762, 2005. 9943, 9944, 9957, 9962, 9967, 9969
- 10 Liu, Y., Wang, Y., Liu, X., Cai, Z., and Chance, K.: Tibetan middle tropospheric ozone minimum in June discovered from GOME observations, *Geophys. Res. Lett.*, 36, L05814, doi:10.1029/2008GL037056, 2009. 9943
- Livesey, N. J., Filipiak, M. J., Froidevaux, L., Read, W. G., Lambert, A., Santee, M. L., Jiang, J. H., Pumphrey, H. C., Waters, J. W., Cofield, R. E., Cuddy, D. T., Daffer, W. H., Drouin, B. J., Fuller, R. A., Jarnot, R. F., Jiang, Y. B., Knosp, B. W., Li, Q. B., Perun, V. S., Schwartz, M. J., Snyder, W. V., Stek, P. C., Thurstans, R. P., Wagner, P. A., Avery, M., Browell, E. V., Cammas, J.-P., Christensen, L. E., Diskin, G. S., Gao, R.-S., Jost, H.-J., Loewenstein, M., Lopez, J. D., Nedelec, P., Osterman, G. B., Sachse, G. W., and Webster, C. R.: Validation of Aura Microwave Limb Sounder O₃ and CO observations in the upper troposphere and lower stratosphere, *J. Geophys. Res.*, 113, D15S02, doi:10.1029/2007JD008805, 2008. 9952
- 20 Livesey, N. J., Read, W. G., Froidevaux, L., Lambert, A., Manney, G. L., Pumphrey, H. C., Santee, M. L., Schwartz, M. J., Wang, S., Cofield, R. E., Cuddy, D. T., Fuller, R. A., Jarnot, R. F., Jiang, J. H., Knosp, B. W., Stek, P. C., Wagner, P. A., and Wu, D. L.: EOS MLS Version 3.3 Level 2 data quality and description document, Tech. rep., Jet Propulsion Laboratory, available at: https://mls.jpl.nasa.gov/data/v3-3_data_quality_document.pdf, 2011. 9947
- 30 Manney, G. L., Hegglin, M. I., Daffer, W. H., Schwartz, M. J., Santee, M. L., and Pawson, S.: Climatology of Upper Tropospheric-Lower Stratospheric (UTLS) jets and tropopauses in MERRA, *J. Climate*, 27, 3248–3271, doi:10.1175/JCLI-D-13-00243.1, 2014. 9965

The Asian monsoon anticyclone in summer 2012

B. Vogel et al.

Title Page

Abstract

Introduction

Conclusions

References

Tables

Figures



Back

Close

Full Screen / Esc

Printer-friendly Version

Interactive Discussion



McKenna, D. S., Grooß, J.-U., Günther, G., Konopka, P., Müller, R., Carver, G., and Sasano, Y.: A new Chemical Lagrangian Model of the Stratosphere (CLaMS): 2. Formulation of chemistry scheme and initialization, *J. Geophys. Res.*, 107, 4256, doi:10.1029/2000JD000113, 2002a. 9945, 9946

5 McKenna, D. S., Konopka, P., Grooß, J.-U., Günther, G., Müller, R., Spang, R., Offermann, D., and Orsolini, Y.: A new Chemical Lagrangian Model of the Stratosphere (CLaMS): 1. Formulation of advection and mixing, *J. Geophys. Res.*, 107, 4309, doi:10.1029/2000JD000114, 2002b. 9945, 9946

Nash, E. R., Newman, P. A., Rosenfield, J. E., and Schoeberl, M. R.: An objective determination of the polar vortex using Ertel's potential vorticity, *J. Geophys. Res.*, 101, 9471–9478, 1996.

10 Pan, L. L., Konopka, P., and Browell, E. V.: Observations and model simulations of mixing near the extratropical tropopause, *J. Geophys. Res.*, 111, D05106, doi:10.1029/2005JD006480, 2006. 9946

15 Pan, L. L., Randel, W. J., Gille, J. C., Hall, W. D., Nardi, B., Massie, S., Yudin, V., Khosravi, R., Konopka, P., and Tarasick, D.: Tropospheric intrusions associated with the secondary tropopause, *J. Geophys. Res.*, 112, D10302, doi:10.1029/2008JD011374, 2009. 9967

Park, M., Randel, W. J., Kinnison, D. E., Garcia, R. R., and Choi, W.: Seasonal variation of methane, water vapor, and nitrogen oxides near the tropopause: Satellite observations and model simulations, *J. Geophys. Res.*, 109, D03302, doi:10.1029/2003JD003706, 2004. 9943, 9969

20 Park, M., Randel, W. J., Gettleman, A., Massie, S. T., and Jiang, J. H.: Transport above the Asian summer monsoon anticyclone inferred from Aura Microwave Limb Sounder tracers, *J. Geophys. Res.*, 112, D16309, doi:10.1029/2006JD008294, 2007. 9943, 9944, 9957

25 Park, M., Randel, W. J., Emmons, L. K., Bernath, P. F., Walker, K. A., and Boone, C. D.: Chemical isolation in the Asian monsoon anticyclone observed in Atmospheric Chemistry Experiment (ACE-FTS) data, *Atmos. Chem. Phys.*, 8, 757–764, doi:10.5194/acp-8-757-2008, 2008. 9943, 9944, 9969

30 Park, M., Randel, W. J., Emmons, L. K., and Livesey, N. J.: Transport pathways of carbon monoxide in the Asian summer monsoon diagnosed from Model of Ozone and Related Tracers (MOZART), *J. Geophys. Res.*, 114, D08303, doi:10.1029/2008JD010621, 2009. 9943, 9944, 9968

Ploeger, F., Günther, G., Konopka, P., Fueglistaler, S., Müller, R., Hoppe, C., Kunz, A., Spang, R., Grooß, J.-U., and Riese, M.: Horizontal water vapor transport in the lower strato-

The Asian monsoon anticyclone in summer 2012

B. Vogel et al.

Title Page

Abstract

Introduction

Conclusions

References

Tables

Figures



Back

Close

Full Screen / Esc

Printer-friendly Version

Interactive Discussion



sphere from subtropics to high latitudes during boreal summer, *J. Geophys. Res.*, 118, 8111–8127, doi:10.1002/jgrd.50636, 2013. 9943, 9964

Ploeger, F., Gottschling, C., Griebbach, S., Grooß, J.-U., Günther, G., Konopka, P., Müller, R., Riese, M., Stroh, F., Ungermann, J., Vogel, B., and von Hobe, M.: On deducing the transport barrier in the Asian summer monsoon anticyclone based on isentropic PV-gradients, *Atmos. Chem. Phys. Discuss.*, submitted, 2015. 9959

Pommrich, R., Müller, R., Grooß, J.-U., Konopka, P., Ploeger, F., Vogel, B., Tao, M., Hoppe, C. M., Günther, G., Spelten, N., Hoffmann, L., Pumphrey, H.-C., Viciani, S., D'Amato, F., Volk, C. M., Hoor, P., Schlager, H., and Riese, M.: Tropical troposphere to stratosphere transport of carbon monoxide and long-lived trace species in the Chemical Lagrangian Model of the Stratosphere (CLaMS), *Geosci. Model Dev.*, 7, 2895–2916, doi:10.5194/gmd-7-2895-2014, 2014. 9946, 9947, 9948

Popovic, J. M. and Plumb, R. A.: Eddy shedding from the upper-tropospheric Asian monsoon anticyclone, *J. Atmos. Sci.*, 58, 93–104, 2001. 9945

Randel, W. J. and Park, M.: Deep convective influence on the Asian summer monsoon anticyclone and associated tracer variability observed with Atmospheric Infrared Sounder (AIRS), *J. Geophys. Res.*, 111, D12314, doi:10.1029/2005JD006490, 2006. 9943, 9945, 9949

Randel, W. J., Park, M., Emmons, L., Kinnison, D., Bernath, P., Walker, K. A., Boone, C., and Pumphrey, H.: Asian monsoon transport of pollution to the stratosphere, *Science*, 328, 611–613, doi:10.1126/science.1182274, 2010. 9943

Riese, M., Ploeger, F., Rap, A., Vogel, B., Konopka, P., Dameris, M., and Forster, P.: Impact of uncertainties in atmospheric mixing on simulated UTLS composition and related radiative effects, *J. Geophys. Res.*, 117, D16305, doi:10.1029/2012JD017751, 2012. 9944, 9970

Rosenlof, K. H., Tuck, A. F., Kelly, K. K., Russell III, J. M., and McCormick, M. P.: Hemispheric asymmetries in the water vapor and inferences about transport in the lower stratosphere, *J. Geophys. Res.*, 102, 13213–13234, 1997. 9943, 9944, 9969

Sander, S. P., Friedl, R. R., Barker, J. R., Golden, D. M., Kurylo, M. J., Wine, P. H., Abbatt, J. P. D., Burkholder, J. B., Kolb, C. E., Moortgat, G. K., Huie, R. E., and Orkin, V. L.: Chemical Kinetics and Photochemical Data for Use in Atmospheric Studies, JPL Publication, 10-6, 2011. 9947

Schwartz, M. J., Manney, G. L., Hegglin, M. I., Livesey, N. J., Santee, M. L., and Dafer, W. H.: Climatology and variability of trace gases in extratropical double-tropopause re-

The Asian monsoon anticyclone in summer 2012

B. Vogel et al.

Title Page

Abstract

Introduction

Conclusions

References

Tables

Figures



Back

Close

Full Screen / Esc

Printer-friendly Version

Interactive Discussion



gions from MLS, HIRDLS and ACE-FTS measurements, *J. Geophys. Res.*, 120, 843–867, doi:10.1002/2014JD021964, 2015. 9967

Shindell, D. T.: Climate and ozone response to increased stratospheric water vapor, *Geophys. Res. Lett.*, 28, 1551–1554, doi:10.1029/1999GL011197, 2001. 9943

5 Smith, C. A., Haigh, J. D., and Toumi, R.: Radiative forcing due to trends in stratospheric water vapour, *Geophys. Res. Lett.*, 28, 179–182, 2001. 9943

Solomon, S., Rosenlof, K., Portmann, R., Daniel, J., Davis, S., Sanford, T., and Plattner, G.-K.: Contributions of stratospheric water vapor to decadal changes in the rate of global warming, *Science*, 327, 1219–1223, doi:10.1126/science.1182488, 2010. 9944, 9970

10 Spang, R., Günther, G., Riese, M., Hoffmann, L., Müller, R., and Griessbach, S.: Satellite observations of cirrus clouds in the Northern Hemisphere lowermost stratosphere, *Atmos. Chem. Phys.*, 15, 927–950, doi:10.5194/acp-15-927-2015, 2015. 9964

Uma, K. N., Das, S. K., and Das, S. S.: A climatological perspective of water vapor at the UTLS region over different global monsoon regions: observations inferred from the Aura-MLS and reanalysis data, *Clim. Dynam.*, 43, 407–420, doi:10.1007/s00382-014-2085-9, 2014. 9943

15 Vernier, J.-P., Thomason, L. W., and Kar, J.: CALIPSO detection of an Asian tropopause aerosol layer, *Geophys. Res. Lett.*, 38, L07804, doi:10.1029/2010GL046614, 2011. 9943

Vogel, B., Konopka, P., Grooß, J.-U., Müller, R., Funke, B., López-Puertas, M., Reddman, T., Stiller, G., von Clarmann, T., and Riese, M.: Model simulations of stratospheric ozone loss caused by enhanced mesospheric NO_x during Arctic Winter 2003/2004, *Atmos. Chem. Phys.*, 8, 5279–5293, doi:10.5194/acp-8-5279-2008, 2008. 9946

20 Vogel, B., Feck, T., and Grooß, J.-U.: Impact of stratospheric water vapor enhancements caused by CH₄ and H₂ increase on polar ozone loss, *J. Geophys. Res.*, 116, D05301, doi:10.1029/2010JD014234, 2011a. 9944, 9948

25 Vogel, B., Pan, L. L., Konopka, P., Günther, G., Müller, R., Hall, W., Campos, T., Pollack, I., Weinheimer, A., Wei, J., Atlas, E. L., and Bowman, K. P.: Transport pathways and signatures of mixing in the extratropical tropopause region derived from Lagrangian model simulations, *J. Geophys. Res.*, 116, D05306, doi:10.1029/2010JD014876, 2011b. 9946, 9967

Vogel, B., Feck, T., Grooß, J.-U., and Riese, M.: Impact of a possible future global hydrogen economy on Arctic stratospheric ozone loss, *Energ. Environ. Sci.*, 5, 6445–6452, doi:10.1039/c2ee03181g, 2012. 9944

30 Vogel, B., Günther, G., Müller, R., Grooß, J.-U., Hoor, P., Krämer, M., Müller, S., Zahn, A., and Riese, M.: Fast transport from Southeast Asia boundary layer sources to northern Europe:

rapid uplift in typhoons and eastward eddy shedding of the Asian monsoon anticyclone, *Atmos. Chem. Phys.*, 14, 12745–12762, doi:10.5194/acp-14-12745-2014, 2014. 9943, 9951, 9952, 9954, 9957, 9958, 9962, 9964, 9967, 9969

- 5 Xiong, X., Houweling, S., Wei, J., Maddy, E., Sun, F., and Barnet, C.: Methane plume over south Asia during the monsoon season: satellite observation and model simulation, *Atmos. Chem. Phys.*, 9, 783–794, doi:10.5194/acp-9-783-2009, 2009. 9943, 9969
- Yan, R.-C., Bian, J.-C., and Fan, Q.-J.: The impact of the South Asia High Bimodality on the chemical composition of the upper troposphere and lower stratosphere, *Atmos. Ocean. Sci. Lett.*, 4, 229–234, 2011. 9945, 9953, 9954
- 10 Zhang, Q., Wu, G., and Qian, Y.: The Bimodality of the 100 hPa South Asia high and its relationship to the climate anomaly over East Asia in summer, *J. Meteorol. Soc. Jpn.*, 80, 733–744, 2002. 9945, 9953, 9954, 9968

ACPD

15, 9941–9995, 2015

The Asian monsoon anticyclone in summer 2012

B. Vogel et al.

[Title Page](#)[Abstract](#)[Introduction](#)[Conclusions](#)[References](#)[Tables](#)[Figures](#)[Back](#)[Close](#)[Full Screen / Esc](#)[Printer-friendly Version](#)[Interactive Discussion](#)

The Asian monsoon anticyclone in summer 2012

B. Vogel et al.

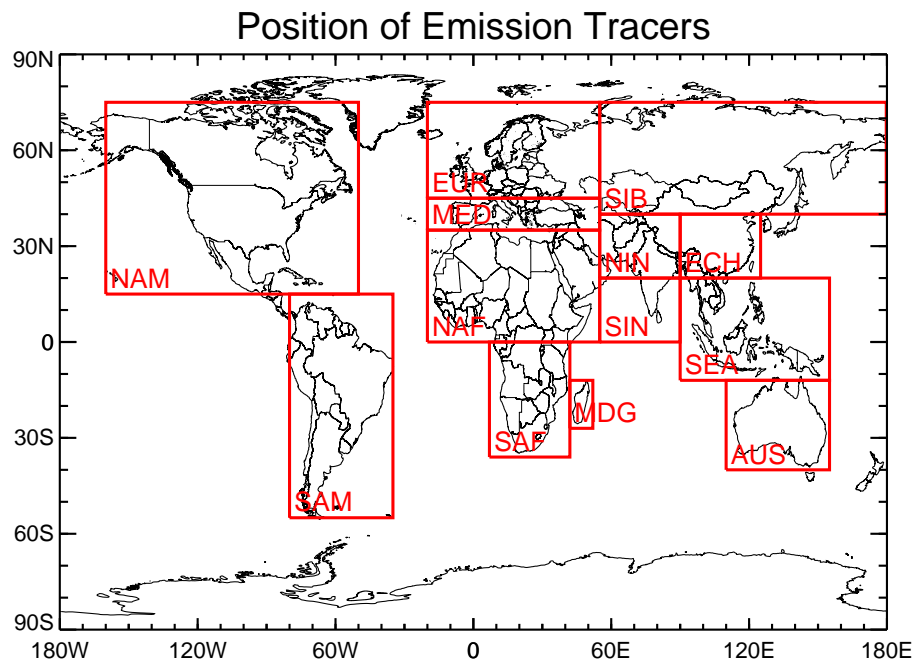


Figure 1. Global geographic position of artificial boundary layer source regions in the CLAMS model, also referred to as “emission tracers”. The latitude and longitude range for each emission tracer is listed in Table 1.

Title Page

Abstract

Introduction

Conclusions

References

Tables

Figures



Back

Close

Full Screen / Esc

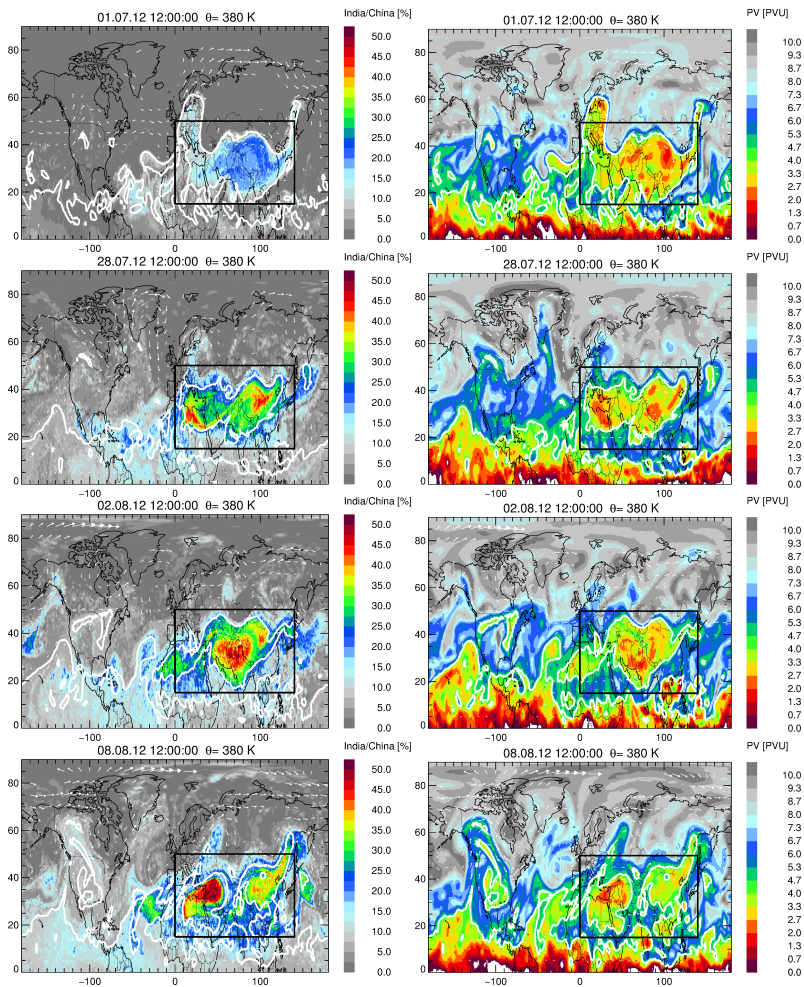
Printer-friendly Version

Interactive Discussion



The Asian monsoon anticyclone in summer 2012

B. Vogel et al.



Title Page	
Abstract	Introduction
Conclusions	References
Tables	Figures
◀	▶
◀	▶
Back	Close
Full Screen / Esc	
Printer-friendly Version	
Interactive Discussion	



The Asian monsoon anticyclone in summer 2012

B. Vogel et al.

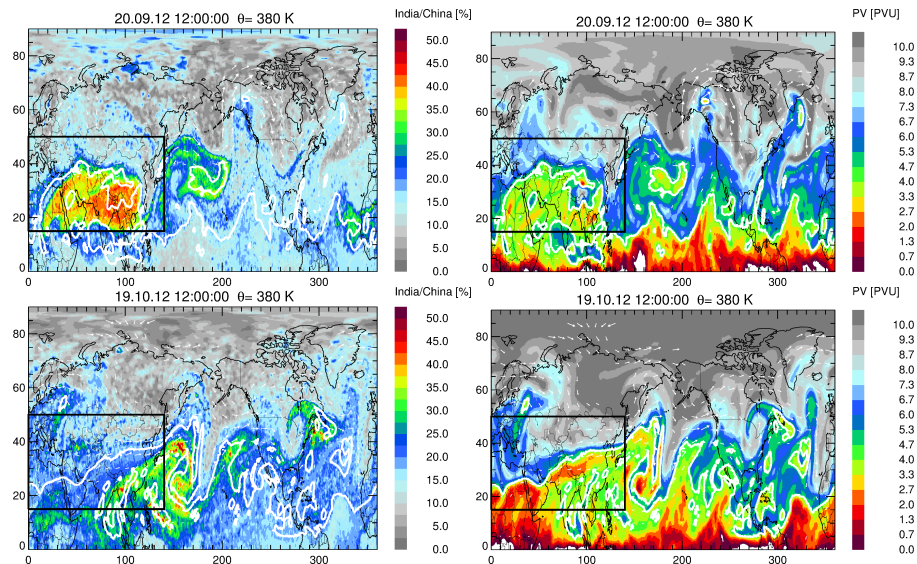


Figure 3. The same as Fig. 2, but on 20 September 2012 (top) and on 19 October 2012 (bottom). Here for simplification, the abscissa is for the longitude range from 0 to 360° to highlight the eddy shedding event on 20 September 2012 (top) and the distribution of emission tracers for India/China after the breakup of the anticyclone on 19 October 2012 (bottom).

Title Page

Abstract

Introduction

Conclusions

References

Tables

Figures

◀

▶

◀

▶

Back

Close

Full Screen / Esc

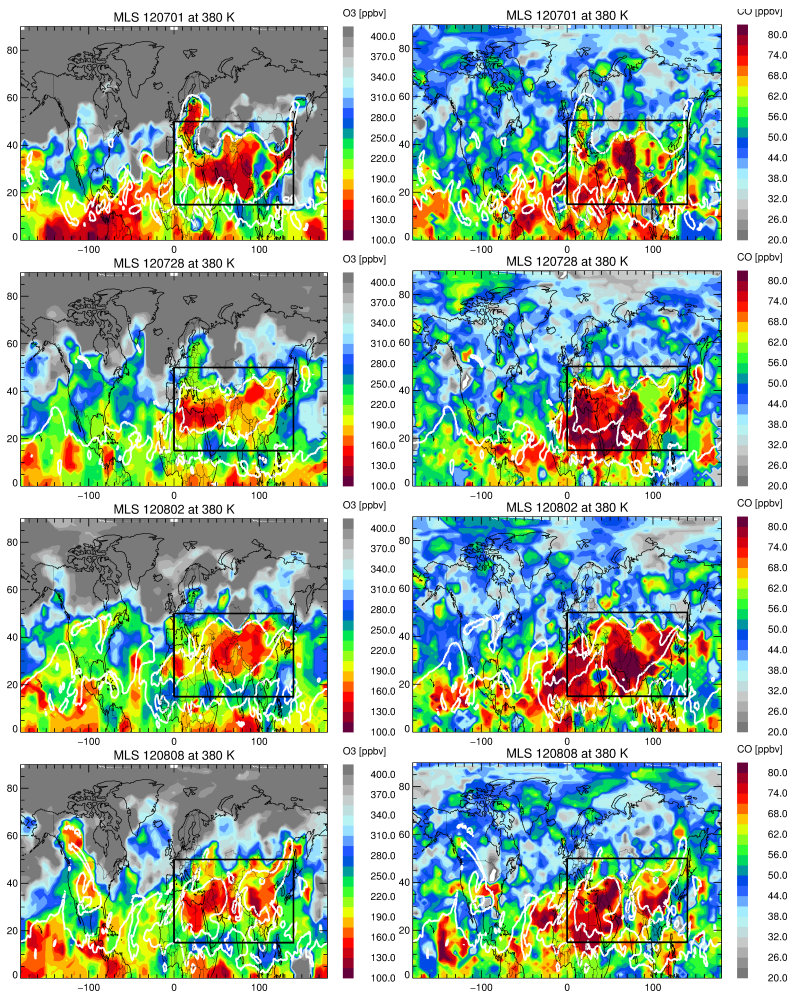
Printer-friendly Version

Interactive Discussion



The Asian monsoon anticyclone in summer 2012

B. Vogel et al.


[Title Page](#)
[Abstract](#)
[Introduction](#)
[Conclusions](#)
[References](#)
[Tables](#)
[Figures](#)

[Back](#)
[Close](#)
[Full Screen / Esc](#)
[Printer-friendly Version](#)
[Interactive Discussion](#)


The Asian monsoon anticyclone in summer 2012

B. Vogel et al.

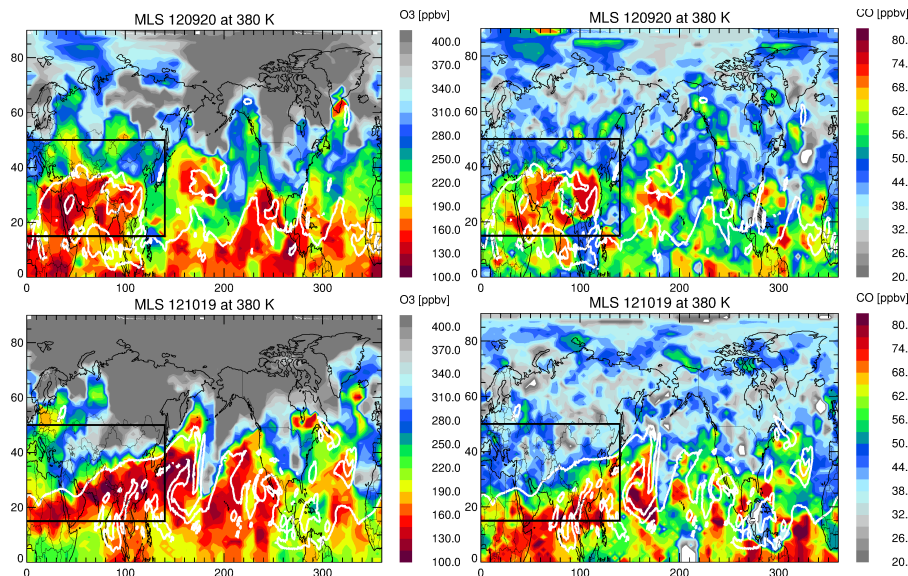


Figure 5. The same as Fig. 4, but on 20 September 2012 (top) and on 19 October 2012 (bottom). Here for simplification, the abscissa is for the longitude range from 0 to 360° to highlight the distribution of O₃ and CO during the eddy shedding event on 20 September 2012 (top) and after the breakup of the anticyclone on 19 October 2012 (bottom).

[Title Page](#)[Abstract](#)[Introduction](#)[Conclusions](#)[References](#)[Tables](#)[Figures](#)[◀](#)[▶](#)[◀](#)[▶](#)[Back](#)[Close](#)[Full Screen / Esc](#)[Printer-friendly Version](#)[Interactive Discussion](#)

The Asian monsoon anticyclone in summer 2012

B. Vogel et al.

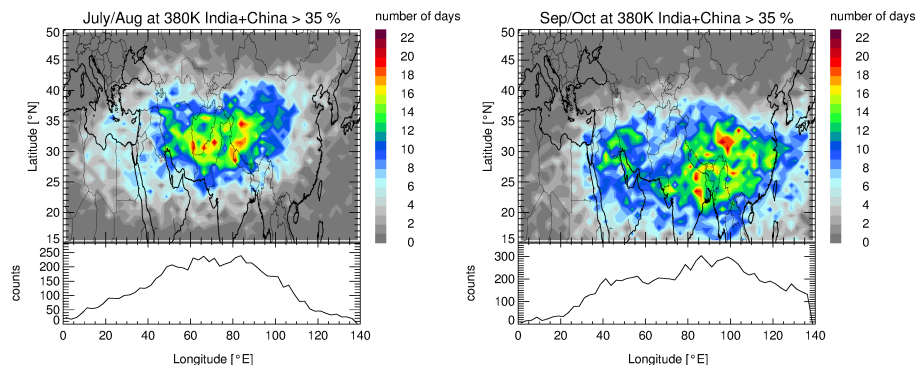
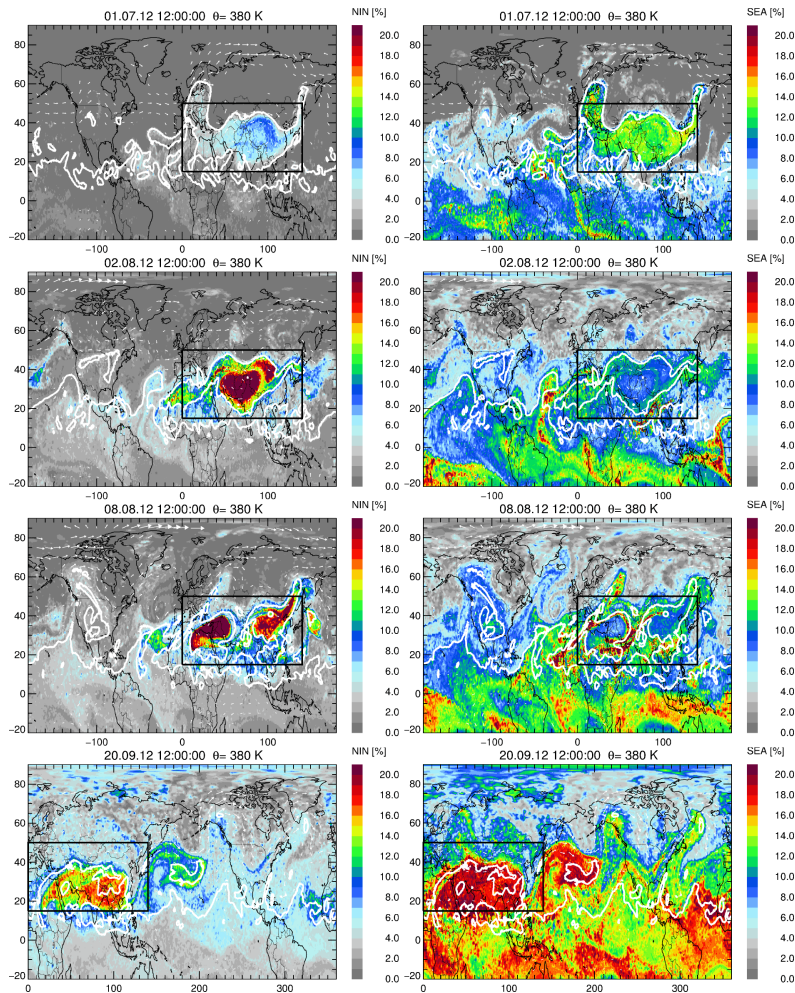


Figure 6. The number of days ($N(\lambda, \phi)$) (top panel) calculated in latitude-longitude bins (of 2.5° longitude \times 1.0° latitude) at 380 K (± 1 K) with mean values of the contributions of emission tracers for India/China larger than 35% for July/August (left) and September/October (right) 2012. The longitudinal dependence (bottom panel) of the occurrence of days with contributions of emission tracers for India/China larger than 35% (here “counts” is the number of days summarised over all latitude bins for one longitude bin: $\text{counts}(\phi) = \sum_{\lambda=15^\circ}^{\lambda=50^\circ} N(\phi)$).

[Title Page](#)
[Abstract](#)
[Introduction](#)
[Conclusions](#)
[References](#)
[Tables](#)
[Figures](#)

[Back](#)
[Close](#)
[Full Screen / Esc](#)
[Printer-friendly Version](#)
[Interactive Discussion](#)

The Asian monsoon anticyclone in summer 2012

B. Vogel et al.

Title Page

Abstract Introduction

Conclusions References

Tables Figures

◀ ▶

◀ ▶

Back Close

Full Screen / Esc

Printer-friendly Version

Interactive Discussion



The Asian monsoon anticyclone in summer 2012

B. Vogel et al.

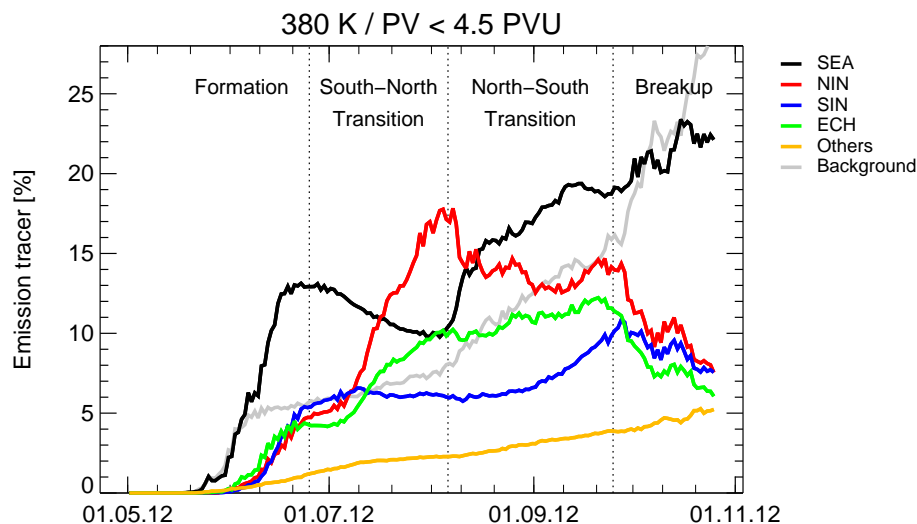


Figure 8. Temporal evolution of different emissions tracers from Southeast Asia (SEA, black), North India (NIN, red), South India (SIN, blue), East China (ECH, green), and from all other land masses (others, yellow) within the Asian monsoon anticyclone at 380 K from May 2012 until end of October 2012. Contributions of boundary sources not considered in the defined emissions tracers listed in Table 1 are summarised as background (grey). The shown percentages are mean values calculated for air masses in Asia in the region between 15 and 50° N and 0 and 140° E at 380 ± 0.5 K (see black box in Fig. 7) with PV values lower than 4.5 PVU that marks the edge of the anticyclone.

Title Page

Abstract

Introduction

Conclusions

References

Tables

Figures



Back

Close

Full Screen / Esc

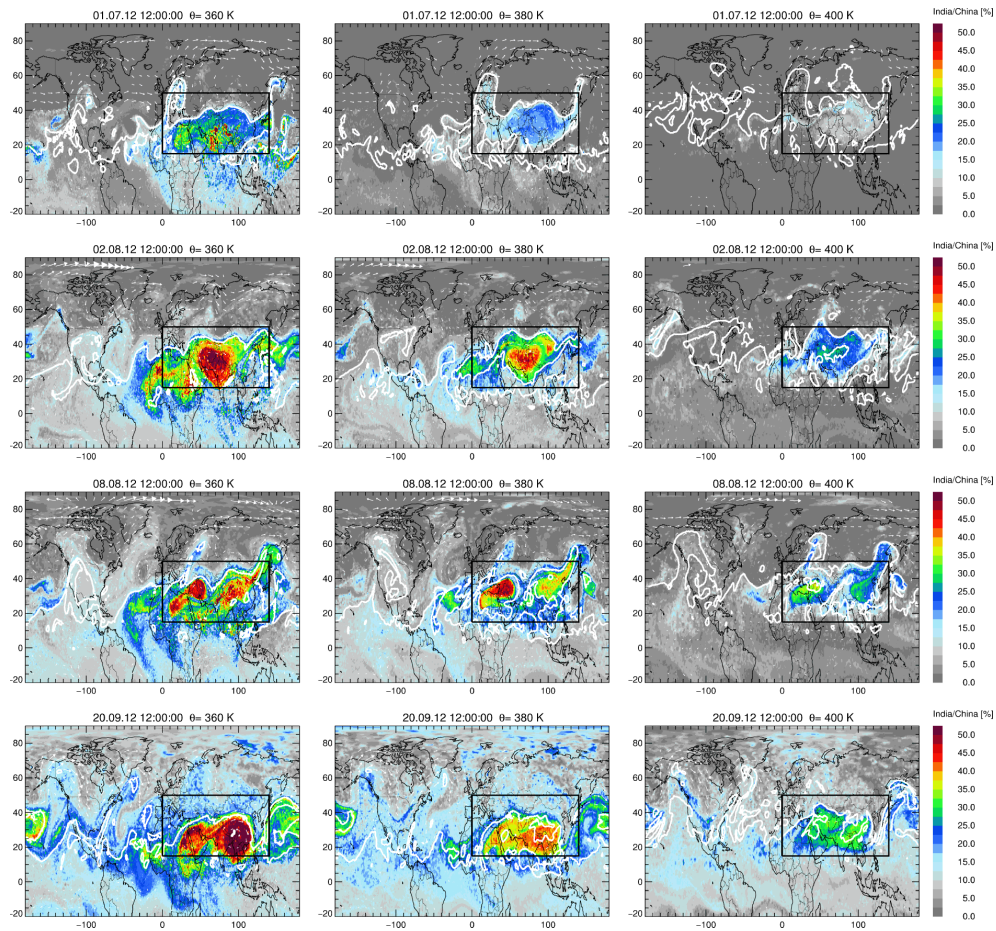
Printer-friendly Version

Interactive Discussion



The Asian monsoon anticyclone in summer 2012

B. Vogel et al.



Title Page

Abstract

Introduction

Conclusions

References

Tables

Figures

◀

▶

◀

▶

Back

Close

Full Screen / Esc

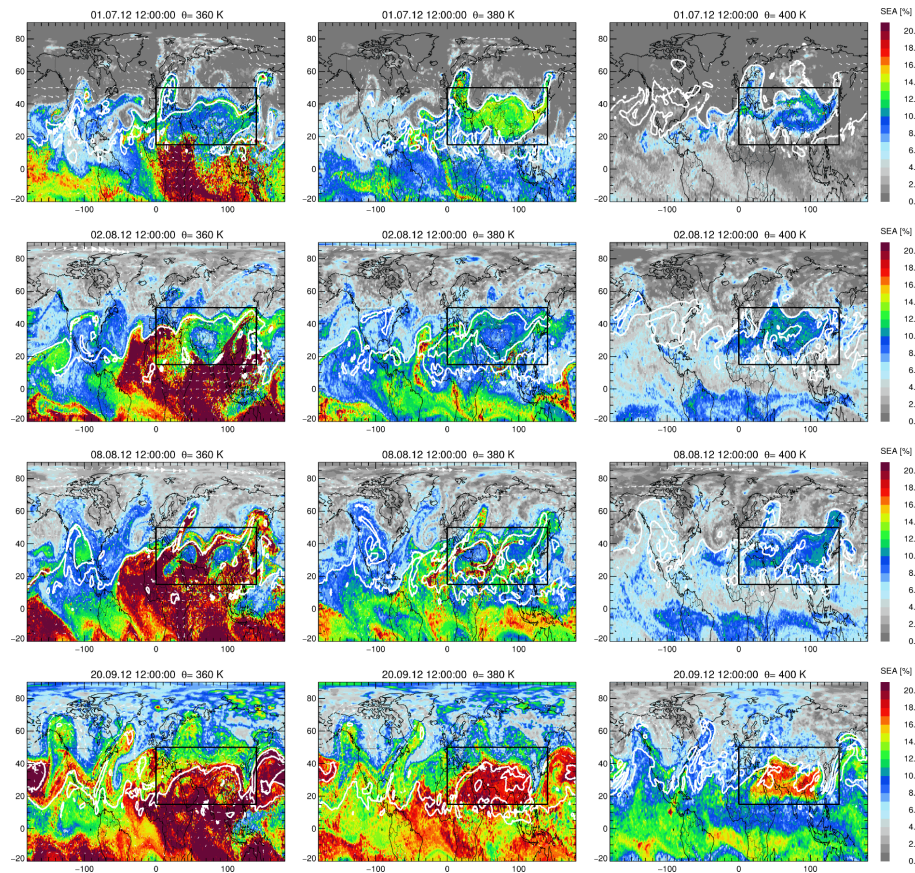
Printer-friendly Version

Interactive Discussion



The Asian monsoon anticyclone in summer 2012

B. Vogel et al.



Title Page	
Abstract	Introduction
Conclusions	References
Tables	Figures
◀	▶
◀	▶
Back	Close
Full Screen / Esc	
Printer-friendly Version	
Interactive Discussion	



The Asian monsoon anticyclone in summer 2012

B. Vogel et al.

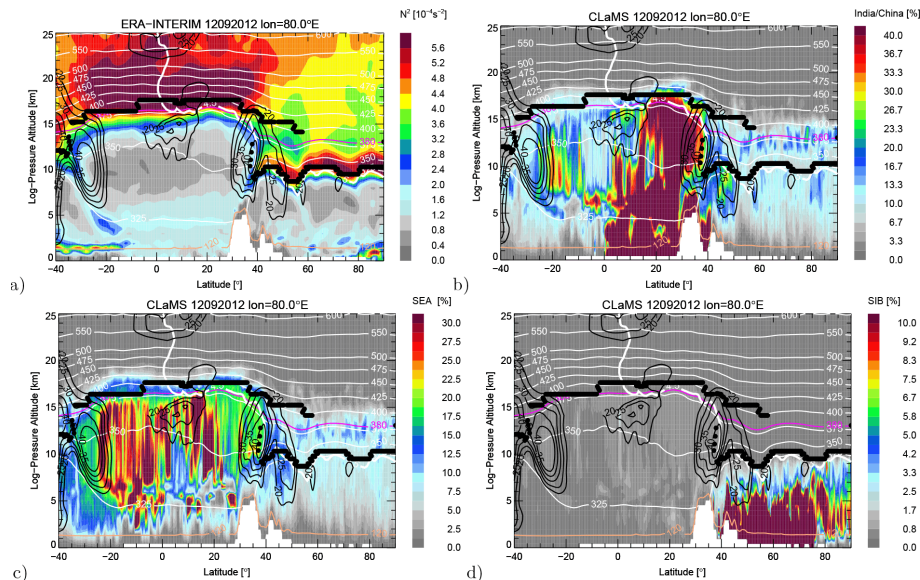


Figure 11. Latitude-height cross-section of the Northern Hemisphere including the Asian Monsoon area ($\approx 15\text{--}35^\circ\text{N}$) at 80°E longitude of (a) static stability (N^2), (b) the fraction of air originating in India/China (here the sum of North India (NIN), South India (SIN), and East China (ECH)), the fraction of air originating in (c) Southeast Asia (SEA) and in (d) Siberia (SIB). The corresponding levels of potential temperature are marked by thin white lines. The 380 K surface is highlighted in purple to illustrate the position of the horizontal cross-sections shown in Figs. 3 and 7. Further, the thermal tropopause (black dots) and the 4.5 PVU surface (thick white lines) are shown. The wind velocities are shown as black lines. The different emission tracers are initialised 2–3 km above surface following orography indicated by the orange line (corresponding to ζ lower than 120 K).